HongTao Wang[1], ShiChao Li[1,2], LingYu Zhang[3], ZheRen Zhao[1], XiaoPeng Yang[1], and YaDong Wang[4]

[1]*College of Earth Sciences, Jilin University, Changchun 130061, P.R. China*

[2]*Key Laboratory of Mineral Resources Evaluation in Northeast Asia, Ministry of Natural Resources, Changchun 130061, P.R. China*

[3]*Department of Geosciences and Natural Resource Management, University of Copenhagen, Copenhagen 1350, Denmark*

[4]*Northwest Institute of Eco-Environment and Resources Chinese Academy of Sciences Lanzhou 730000, P.R. China*

Correspondence to: S-C. Li (`lsc@jlu.edu.cn`)

Key Points:

- The Greater Khingan Mountains in China have experienced two rapid exhumation events and one warming event since the Early Cretaceous.
- The modeling results of a Pecube are highly consistent with the cooling events revealed by thermal history simulation.
- The basin-mountain coupling system of The Greater Khingan Mountain in China is analyzed, and the regional tectonic background is discussed.

Abstract

Apatite fission-track (AFT) tests of clastic samples from the Greater Khingan Mountains (GKM) in China show a center age of 260–62 Ma. Thermal modeling of observed fission-track-length distributions shows three stages of rapid cooling that may have been caused by extensions between 130 and 94 Ma, 30 and 15.3 Ma, and 45 and 0 Ma, and a heating event that may have been caused in part by changes in the subduction direction of the Pacific plate between 64 and 45 Ma. The cumulative exhumation since the Early Cretaceous, is approximately 3 km. The steady-state terrain model in the three-dimensional numerical simulation is highly consistent with the time and rate of the two-dimensional thermal history simulation for the Early Cretaceous exhumation event. The cooling age clusters of ~160 to 100 Ma are similar in the GKM and Hailar-Erlian Basins. This correlation provides a basin–mountain link for the two tectonic domains. Such a basin–mountain coupling lasted through 100–42 Ma, as supported again by the shared cooling ages of samples from the GKM and detritus from the range-bounded basins on the two sides of the mountain range. We interpreted the 130–94 Ma cooling event recorded in the GKM as a result of crustal thickening in response to the closure of the Mongolia-Okhotsk Ocean. An increase in the subduction velocity of the Pacific plate since ca. 45 Ma may have created a post-arc extensional tectonic setting that has prevailed to the present in the GKM.

Plain Language Summary

We reconstructed the thermal evolution history of the region since the Early Cretaceous by tracing the time and temperature evolution of apatite minerals in clastic rocks in the middle part of the Greater Khingan Mountains in China. Two-dimensional (2D) thermal history simulation (HeFty) shows that the Greater Khingan Mountains underwent two periods of rapid exhumation and one period of heating since the Early Cretaceous. We also verified the starting and ending points of the early Cretaceous exhumation events using three-dimensional (3D) thermodynamic simulation (Pecube), and found that the steady-state terrain model in 3D modeling was highly consistent with the results of the HeFty simulation. In addition, we also analyzed the coupling mechanism of the basin-mountain system composed of the Greater Khingan Mountains and the basins on both sides, and concluded that the basin-mountain system began to co-evolve as a whole at about 100 Ma. Since the Early Cretaceous, the Greater Khingan Mountains in China have been exposed under the extensional tectonic setting. During 130–94 Ma, the Greater Khingan Mountains were affected by the closure of the Mongolian-Okhotsk Ocean, and 45 Ma, the Greater Khingan Mountains were affected by the subduction of the Pacific plate under the Eurasian plate.

1 Introduction

The NNE-trending Greater Khingan Mountain range in Northeast China marks the most prominent gravity-anomaly gradient zone across which the crustal thickness decreases rapidly from west to east (Ma, 1987). The current topography of the Greater Khingan Mountains has been generated mainly by tectonic stresses transmitted from the subduction of the Mongolia-Okhotsk Ocean in the north and the Pacific Ocean in the east since the Early Mesozoic (Eizenhöfer et al., 2014; Chen et al., 2017; Liu et al., 2017). The development of the mountain range is considered to have been closely associated with the formation of the Hailar, Erlian, and Songliao basins to the west and east of the Greater Khingan Mountains (Yang et al., 2015; Zhang et al., 2017).

As a dominant orogenic belt in Northeast Asia, the Greater Khingan Mountains recorded far-field responses of plate-boundary processes generated by the evolution of the Mongolia-Okhotsk Ocean and the Pacific Ocean throughout the Phanerozoic. Because of its intracontinental setting, the region is ideal for quantifying the far-field effect of intraplate tectonism (Reiners et al., 2003; Hu et al., 2006). Previous thermal history simulations of apatite studies of the Greater Khingan Mountains area have led to diverse views on the cooling history and tectonic causes of the Greater Khingan mountain building. One view is that the exhumation of the Greater Khingan region did not start until the beginning of the Cenozoic (Fang et al., 2005). Another view is that the exhumation of the mountain range started as early as the Late Mesozoic and extended into the Cenozoic (Li et al., 2011). Wu et al. (2016) inferred that the Mesozoic and Cenozoic cooling events were clustered in the Cretaceous (120–90 Ma) and the Cenozoic since ca. 60 Ma. In contrast, Pang et al. (2020) suggested that the

Greater Khingan Mountains have experienced two episodes of rapid exhumation at ca. 100–60 Ma and ca. 50–0 Ma with a regional reheating event at ca. 60–50 Ma in between. Additionally, Shao et al. (2005) proposed that the exhumation of the Greater Khingan Mountains was driven by mantle upwelling, while other scholars consider that the Greater Khingan Mountains were created by the combined and interactive effect of the subduction of the Mongolia-Okhotsk and Pacific Oceans expressed by back-arc extension (Meng, 2003; Wang et al., 2006; Pang et al., 2020) or the result of only the Pacific Ocean subduction (Li et al., 2011; Wu et al., 2016; Pang et al., 2020). Finally, focused studies on the Greater Khingan Mountains and their neighboring Songliao and Hailar-Erlian basins have been conducted (Fang et al., 2005; Li et al., 2011; Wu et al., 2016; Pang et al., 2020), but the basin-mountain coupling relationship has never been clearly established. In this study, we address the above issues by conducting apatite fission-track (AFT) analysis and three-dimensional (3D) numerical simulation of sedimentary rocks from the central part of the Greater Khingan Mountains using well-established methods for inferring the thermal history of the region (Gallagher et al., 1998; Donelick, 2005; Stockli, 2005; Ketcham et al., 2009; Szymanski et al., 2016).

Figure. 1

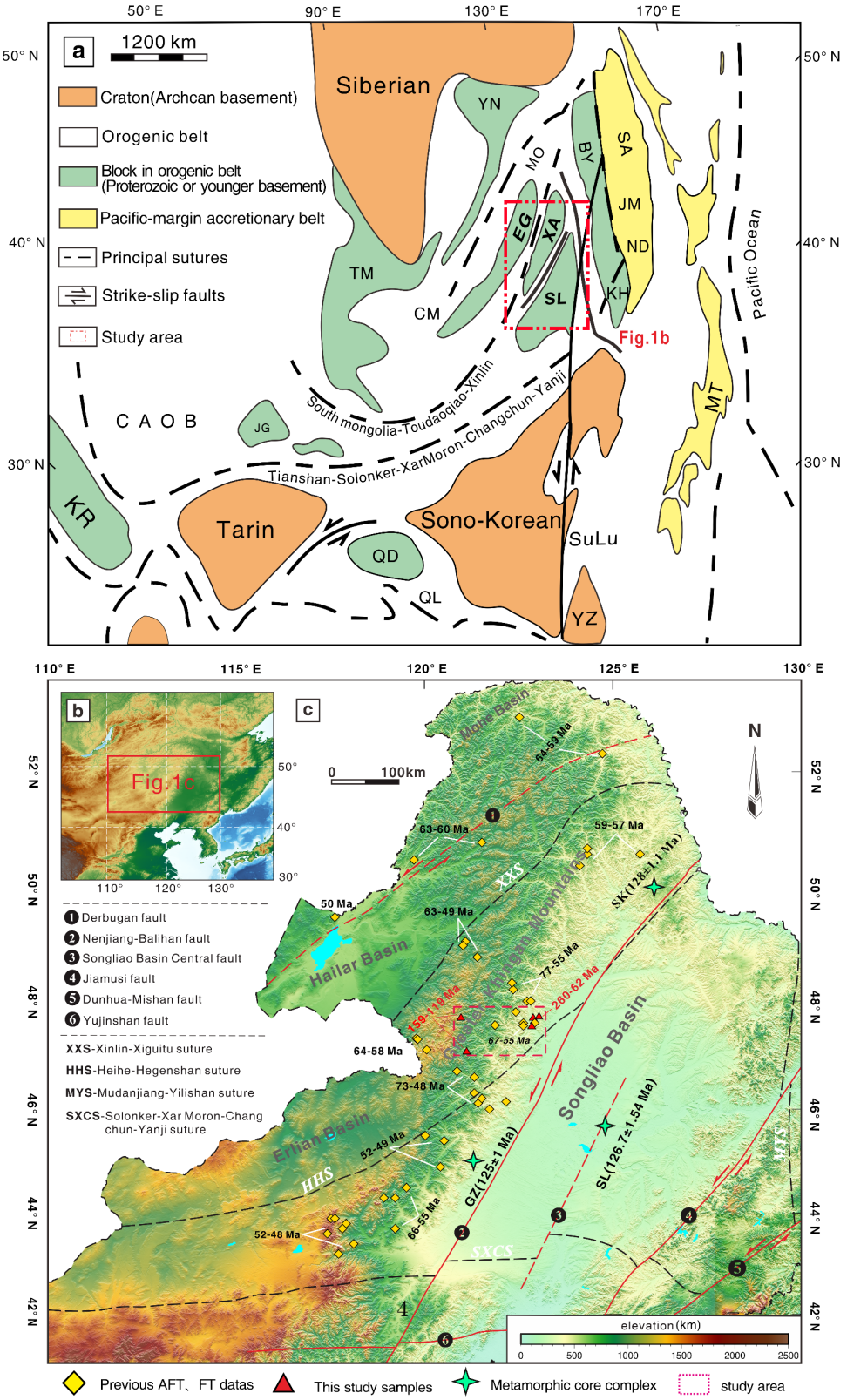
a
1200 km
Craton(Archcan basement)
Orogenic belt
Block in orogenic belt (Proterozoic or younger basement)
Pacific-margin accretionary belt
Principal sutures
Strike-slip faults
Study area
Siberian
YN
MO
BY
SA
JM
ND
KH
EG
XA
SL
TM
CM
Fig.1b
Pacific Ocean
MT
C A O B
JG
South mongolia-Toudaoqiao-Xinlin
Tianshan-Solonker-XarMoron-Changchun-Yanji
KR
Tarin
QD
QL
Sono-Korean
SuLu
YZ
50° E
90° E
130° E
170° E
50° N
40° N
30° N
b
Fig.1c
c
0 100km
N
Mohe Basin
64-59 Ma
63-60 Ma
59-57 Ma
SK(128±1.1 Ma)
XXS
Great Khingan Mountains
50 Ma
63-49 Ma
Hailar Basin
77-55 Ma
260-62 Ma
59-113 Ma
67-55 Ma
64-58 Ma
73-48 Ma
Songliao Basin
SL(126.7±1.54 Ma)
Erlian Basin
52-49 Ma
HHS
GZ(125±1 Ma)
MYS
66-55 Ma
52-48 Ma
SXCS
elevation (km)
0 500 1000 1500 2000 2500
1 Derbugan fault
2 Nenjiang-Balihan fault
3 Songliao Basin Central fault
4 Jiamusi fault
5 Dunhua-Mishan fault
6 Yujinshan fault
XXS-Xinlin-Xiguitu suture
HHS-Heihe-Hegenshan suture
MYS-Mudanjiang-Yilishan suture
SXCS-Solonker-Xar Moron-Chang chun-Yanji suture
Previous AFT、FT datas
This study samples
Metamorphic core complex
study area

Figure 1. (a) Schematic diagram of the main structural units and the location of the study area in Northeast China; CAOB: Central Asian Orogenic Belt, KR: Karakorum, JG: Jungger, TM: Tuva-Mongolia, CM: Central Mongolia, YN: Yablanov, Mo: Mongolia-Okhotsk Ocean, EG: Erguna, XA: Xing'an, SL: Songliao, BY: Bureya, SA: Sikhote-Alin, JM: Jiamusi, ND: Nadanhade, KH: Khanka, MT: Mino-Tamba, YZ: Yangtze, QD: Qaidam (modified from Li, 2006; Safonova et al., 2009; Safonova et al., 2011). (b) Geological diagram and thermal map of Northeast China Chronological data; rhombus label data from Li et al. (2011) and Pang et al. (2020), triangle label data from this study; SK: Xinkailing (Miao et al., 2004; Zhao et al., 2007; Zeng et al., 2011), GZ: Ganzhuer Temple (Yang et al., 2014), SL: Songliao (Zhang et al., 2000).

2 Regional Geology

Northeast China exposes micro-continental blocks that formed parts of the Paleozoic-Early Mesozoic Paleo-Asia orogenic belt (Şengör et al., 1993; Xiao et al., 2003; Wilde, 2015; Liu et al., 2017). From north to south, these blocks are the Erguna block, the Xing'an block, the Songnen block, and the Jiamusi block (Fig. 1a). These blocks were accreted onto the northern margin of the North China craton during the Late Permian-Middle Triassic initial closure of the western Paleo-Asian Ocean (Li, 2006; Wu et al., 2007; Zhang et al., 2008; Donskaya et al., 2013; Xu et al., 2013). The western Paleo-Asian Ocean was expressed as the Mongolia-Okhotsk Ocean that was closed during the Late Jurassic to the end of the Early Cretaceous (Donskaya et al., 2013; Li et al., 2015; Tang et al., 2016; Liu et al., 2017). The influence of the Pacific subduction has affected the entire Northeast China region since the Early Jurassic with the most profound impact in the Early Cretaceous (Wu et al., 2011; Safonova & Santosh, 2014; Chen et al., 2017).

Figure. 2

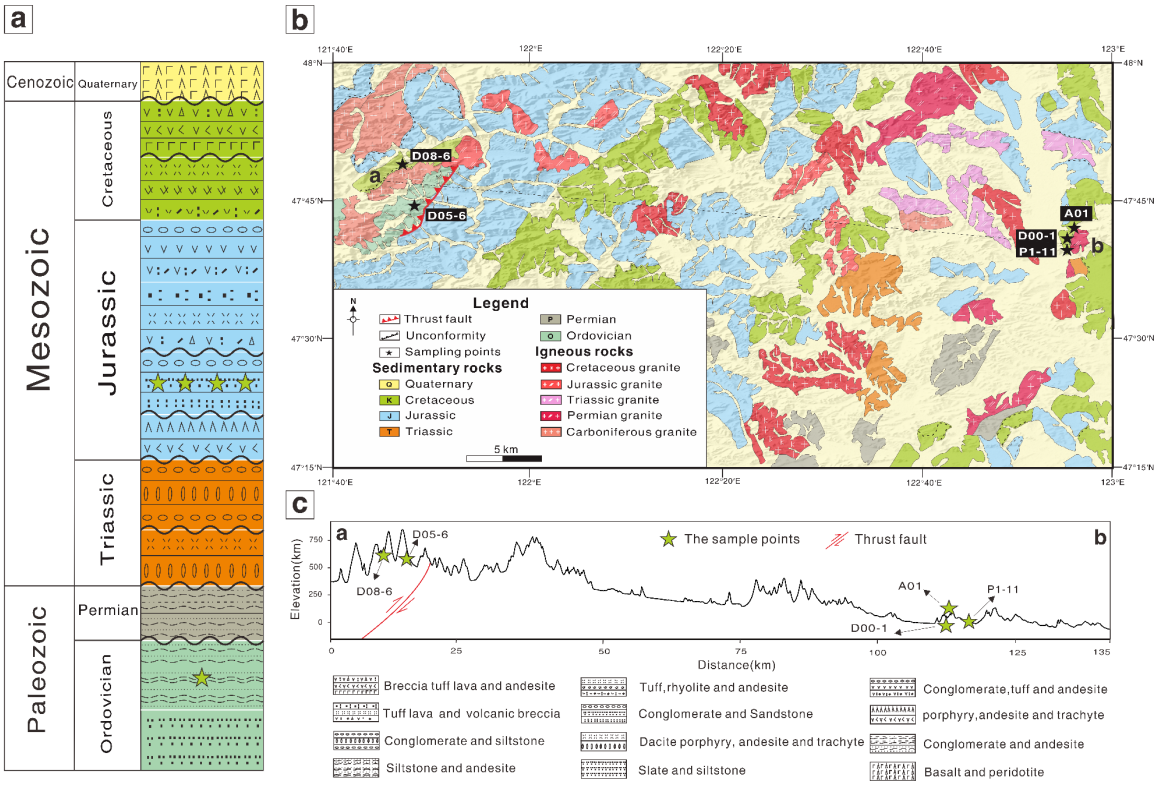

Figure 2. Simplified geological map of the study area and sample locations. (a) Stratigraphic distribution histogram of the study area. (b) Geological map of sampling point locations. (c) Elevation distribution map of sampling points.

3 Data and Methods

The study area is located in the central Greater Khingan Mountains, which form basin-mountain topography with the Hailar-Erlian Basins and Songliao Basin on each side (Fig. 1). The area exposes Ordovician, Permian, Triassic, Jurassic, Cretaceous, and Quaternary sedimentary strata (Fig. 2a, 2b). Upper Jurassic and Lower Cretaceous strata are composed of sandstone and conglomerate beds (Murui Formation) and volcanic rocks (Fig. 2b). To study the exhumation history in the central Greater Khingan Mountains, we took two sandstone samples (A01, P1-11) and two conglomerate (granitic) clast samples (D00-1, D08-6) from the Lower Cretaceous strata (Murui Formation), and one siltstone sample (D05-6) from the Middle and Upper Ordovician Naked He Formation on the hanging wall of the thrusting fault (Fig. 2a, 2b). The altitude of the samples was 259–849 m (Table 1). None of the samples displayed deformation or the effects of magmatic and hydrothermal activities.

Mineral separation was conducted at the Key Laboratory of Mineral Resources

of Western Gansu Province at Lanzhou University. Apatite grains were picked out using standard magnetic separation techniques. Apatite grains were fixed in epoxy resin and polished and then placed in a 5 N HNO_3 solution at 20°C. This was followed by etching for 20 seconds to magnify the spontaneously generated fission tracks. Durango (31.4 ± 0.5 Ma) and Fish Canyon Tuff (27.9 ± 0.7 Ma) apatite grains were used as age standards. The sample, age standard, and IRMM540R dosimeter glass were irradiated in the thermal reactor of Oregon State University with a nominal neutron flux of 9×10^{15} n • cm^{-2}. After irradiation, the mica detector was etched in a 40% HF solution at a temperature of 20°C to magnify the fission tracks induced by neutrons in the apatite particles. The fission trajectory analysis was conducted in the Fission Track Laboratory of the Public Technical Service Center of the Lanzhou Oil and Gas Resource Center of the Chinese Academy of Sciences. The age of fission tracks in all samples was determined using the calibration method (Hurford & Green, 1983), and the individual value in this study was 257.56 ± 17.67.

The D_{par} value is an important index used to quantitatively characterize the solubility of apatite (Donelick et al., 1999). It is the maximum diameter of the fission track etching image parallel to the crystalline C-axis that intersects with the polished surface. The track length and D_{par} value are used to measure the degree of annealing of the sample (Ketcham et al., 2007). We used the chi-square test, P(χ^2test), to analyze the age dispersion of apatite grains: (1) P(χ^2) > 5% indicates that the track age distribution is more concentrated (Galbraith & Laslett, 1993), and (2) P(χ^2) < 5% indicates that the track age distribution is more dispersed. We divided the track ages with P(χ^2) < 5% into different age clusters for use in thermal modeling and geologic interpretations (Stewart & Brandon, 2004). Based on the correlation between the peak ages of the sample models, the peak ages were divided into three groups, namely, P1 (41.9–16.2 Ma), P2 (159–108 Ma), and P3 (378 Ma). The dispersed age distribution may have resulted from younger thermal events or complex chemical compositions of the apatite grains. We used Density Plotter 7.0 (Vermeesch, 2012) to draw the length-frequency distribution of fission-tracks (Fig. 3), and HeFty 1.9.1 for modeling the thermal history using fission-track length, D_{par} value, and C-axis orientation. Based on the obtained apatite fission-track age data and two-dimensional (2D) thermal history inversion results, Pecube 3D numerical simulation inversion and forward modeling (Malcolm & Sambridge 1999; Sambridge 1999; Braun 2003; Braun, et al. 2012) were used to reveal the thermal history of rocks, predict the thermal age of sample data, verify the accuracy of 2D thermal history inversion results, and determine the uplift and exhumation history of the middle Greater Khingan Mountains.

Table 1. Locations, lithology, and stratigraphic ages of samples colleced from the central Greater Khingan Mountain region.

@ >p(- 10) * >p(- 10) * >p(- 10) * >p(- 10) * >p(- 10) * >p(- 10) * @ Sample

number & Location & Lithology & Elevation

(m) & Depositional age (U-Pb)

(Ma) &
& Longitude

(°E) & Latitude

(°N) & & &
D08-6 & 120°55 3 & 47°48 42 & Conglomerate (granitic) & 849 & 147-146 (Li et al., 2015)
P1-11 & 122°51 30.23 & 47°40 27.68 & Sandstone & 297 & 147-146 (Li et al., 2015)
D05-6 & 121°5 49 & 47°42 8 & Siltstone & 765 & 480-460 (Jiang et al., 2018)
D00-1 & 122°51 37.80 & 47°41 36.04 & Conglomerate (granitic) & 259 & 147-146 (Li et al., 2015)
A01 & 122°51 37.80 & 47°41 36.04 & Sandstone & 259 & 147-146 (Li et al., 2015)

4 Results and Thermal History Modeling

4.1 AFT Results

The results of the AFT analysis are shown in Table 2. Three of the five samples (samples P1-11, D00-1, and A01) passed the chi-square test with $P(\chi^2<) < 5\%$. The AFT ages of the samples were scattered, with the center age distributed between 61.8 ± 6.4 Ma and 260 ± 36 Ma, and the average length of the track length between 11.62 ± 1.09 µm and 12.85 ± 2.01 µm. The short track length can be attributed to a strong annealing effect. In addition, we evaluated the effects of D_{par} values on cooling age and fission track length (Figs. S1 and S2). The D_{par} value showed a weak correlation with age, indicating that the annealing process was mainly affected by thermal tectonic events. There was a positive correlation between the D_{par} value and the track length, which is consistent with the theory that the larger the D_{par} value is, the more annealed the sample is.

The fission-track radial graph shows that with the exception of sample D08-6, which had a small apatite sampling size at $N = 7$, the remaining four samples ensured that the track counts were $N > 20$. Samples A01, D00-1, and P1-11 from the Cretaceous Murui Formation exhibited the following features. The single grain ages obtained from A01 and D00-1 were relatively dispersed as indicated by the respective center ages of 107 ± 14 Ma and 61.8 ± 6.4 Ma and track lengths of 12.03 ± 1.8 µm and 11.62 ± 1.09 µm; the track lengths were much shorter than the initial track length of 16.3 ± 0.9 µm (Fig. 3) (Gleadow et al., 1986). The peak split results showed peak ages for A01 ($N = 26$) of 113 ± 11 Ma and 16.2 ± 4.3 Ma and peak ages for D00-1 ($N = 68$) of 108.0 ± 28 Ma and 41.9 ± 5.5 Ma. The peak split results of the sandstone sample P1-11 ($N = 20$) showed apatite ages dispersed between 378 ± 78 Ma and 155 ± 21 Ma, and a central age of 260 ± 36 Ma, which is much older than the age of the

strata from which the samples were collected. The average track length of this sample was 11.92 ± 1.51 µm, which is less than the initial track length of 16.3 ± 0.9 µm (Fig. 3) (Gleadow et al., 1986).

Because sample D08-6 had fewer grains, there was little overlap between the single particle age and the stratigraphic sedimentary age, indicating that it may be composed of older particles and therefore has not been reset. The Ordovician sandstone sample D05-6 (N = 85) taken from the hanging wall of a thrust yielded a concentrated age spread with a center age off 121 ± 10 Ma, which is much younger than the stratigraphic age of the sample (480–460 Ma). The track length of the sample was 12.85 ± 2.01 µm. It is worth noting that the confined track length of sample D05-6 presented a bimodal distribution, indicating that the sample was overheated and overlapped, and the track components were accumulated in two or more thermal events, and the average track length was less than 13 µm (Fig. 3) (Gleadow et al., 1986).

Figure. 3

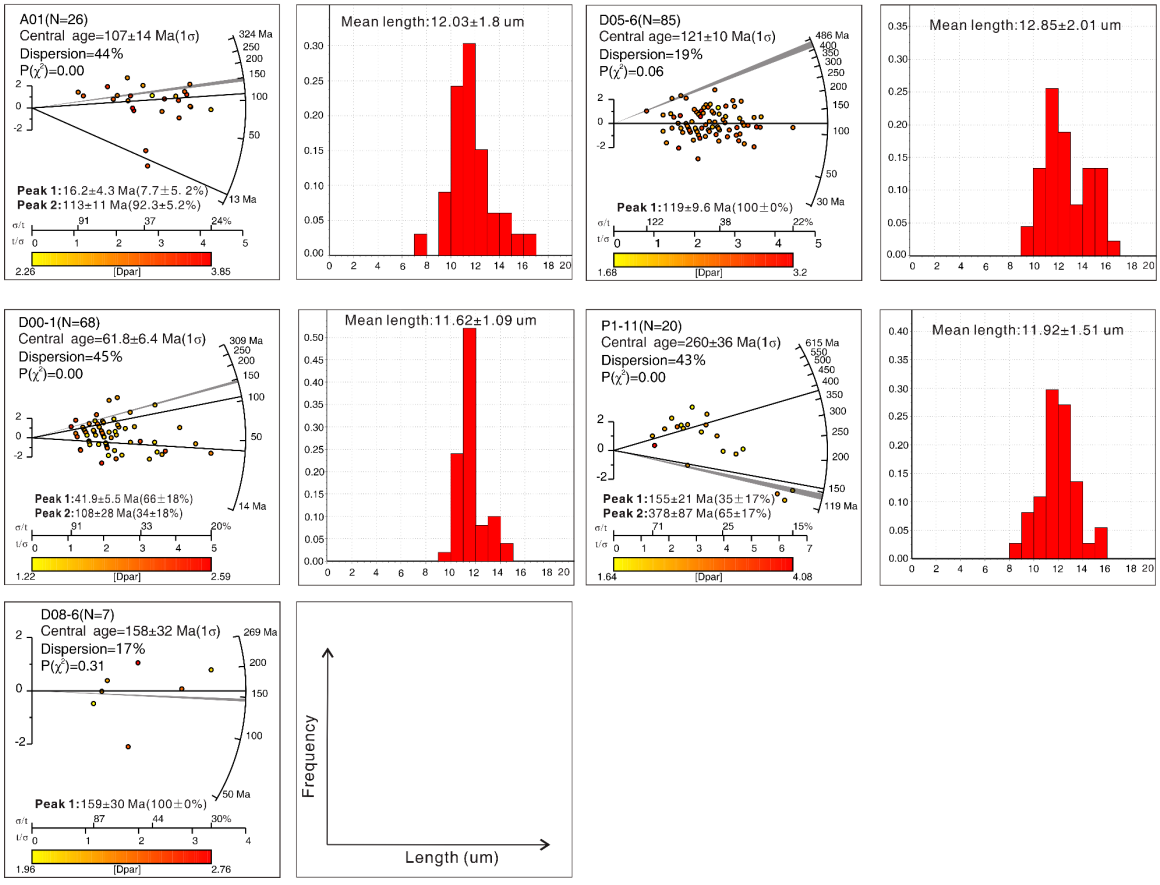

Figure 3. Radial graph of apatite fission-track (AFT) and histogram of confined fission-track length of the sample. The age of the single-particle fission-track is color-coded according to the D_{par} value. N represents the number of particles in the sample; Dispersion represents the discrete value of age; the gray shadows represent the stratigraphic age of the sample; and the black line represents the peak AFT age calculated using the automatic mixing model in RadialPlotter (Vermeesch, 2009). The length histogram shows the relative frequency of the confined track length, with N confined tracks measured.

Table 2. Greater Khingan Mountain apatite fission-track data obtained using the zeta external detector method (Hurford & Green, 1983).

@ >p(- 24) * >p(- 24) * >p(- 24) * >p(- 24) * >p(- 24) * >p(- 24) * >p(- 24) * >p(- 24) * >p(- 24) * >p(- 24) * >p(- 24) * @

Sample number

& No.

grains

(n) & ρ_s (N_s) & ρ_i (N_i) & ρ_d (N_d) & P(χ^2) & Pooled age

(±1)

(Ma) & Central age

(±1)

(Ma) & Mixture model peaks

(±1) (Ma) & MTL

(±1)

(µm)/N & Average D_{par}

(µm) & &
& & & & & & & **P1** & **P2** & **P3** & &
D08-6 & 7 & 5.15(58) & 6.837(77) & 16.6(15655) & 0.31 & 159±30 & 158±32 & N.D.# & 159±30 & N.D.# & N.D.# & 2.32
P1-11 & 20 & 7.352(575) & 7.531(589) & 17.7(15655) & 0 & 218.8±19.8 & 260±36 & N.D.# & 155±21 & 378±87 & 11.92±1.51(37) & 2.34
D05-6 & 85 & 3.729(836) & 6.718(1506) & 16.8(15655) & 0.06 & 119±9.7 & 121±10 & N.D.# & 119±9.6 & N.D.# & 12.85±2.01(94) & 2.49
D00-1 & 68 & 4.55(489) & 19.882(2137) & 17.9(15655) & 0 & 52.5±4.5 & 61.8±6.4 & 41.9±5.5 & 108±28 & N.D.# & 11.62±1.09(50) & 1.74
A01 & 26 & 6.981(327) & 17.614(825) & 17.2(15655) & 0 & 87.2±8.3 & 107±11 & 16.2±4.3 & 113±11 & N.D.# & 12.03±1.8(33) & 3.17
Notes: No. grains – number of grains measured in each sample; ρ_s (N_s) – spontaneous track density (number of spontaneous tracks); ρ_d (N_d) – the induction track density in the outer detector adjacent to the glass dosimeter (the induction track density in the external detector adjacent to the glass dosimeter);

$P(\chi^2)$— − chi-square probability (Galbraith & Laslett, 1993); Pooled age and Central age − represent the pool age of the sample (Vermeesch, 2012) and the central and peak ages of the sample (Vermeesch, 2009); MTL − average length of confined track; Dpar − maximum track length parallel to the crystal C-axis on the intersecting polished surface.

*Durango apatite samples are used as the calibration standard.

†Ages determined by external detector method using zeta values of 257.56 ± 17.67 for apatite.

#N.D.= not determined. & & & & & & & & & & & &

4.2 Thermal History Modeling

AFT ages and short track lengths were distributed discretely (Fig. 3 and Table 2), indicating that the sample itself does not directly indicate the cooling time experienced by the study area, and that the study area has experienced multiple complex exhumation cooling events. Thus, thermal history simulations were conducted. For this, we selected the samples (A01, D00-1, D05-6) that experienced severe annealing in the formation causing partial reset, and used HeFty1.9.1 software (Ketcham et al., 2007, 2009).

In the Cretaceous period, the geothermal gradient in Songliao Basin exceeded 30°C/km (Luo et al., 2017; Wang et al., 2019). Therefore, in the thermal history simulation, the geothermal gradient in the Greater Khingan Mountains was set to 35°C/km (Li et al., 2011), and the surface temperature was set to 15 ± 15°C. Based on previous studies and regional geological data, the thermal history of samples that were used for thermal history simulation was constrained as follows: (1) The initial conditions of the simulation were set at 1.5–2 times the central age of the samples, and the initial burial temperature of the simulation at 20 ± 15°C. The sedimentary age of the syntectonic sedimentary Murui Formation is about 150 Ma (Li et al., 2015), and it is in contact with the underlying Tamulangou formation fault, revealing the active tectonic background at that time, which indicates that the formation of the Murui Formation experienced a process of rapid burial depth and compaction diagenesis after receiving sedimentation. The single particle age of samples A01 and D00-1 from the Murui Formation is partially greater than the formation age, retaining the cooling information of the provenance area. Therefore, the initial constraints set for the thermal history simulation are reasonable. (2) The three samples simulated by thermal history have a similar peak age of about 119–108 Ma (Fig. 3), and the single particle age of the samples is centrally distributed in this time period (Fig. 5). Therefore, the second constraint of the simulation was set to about 120°C when the sample enters the partial annealing zone of wollastonite at about the peak age of each sample. (3) Based on the published data of Pang et al. (2020), the sample is considered to have experienced burial depth heating between 60 and 50 Ma. Inversion ceases once 200 well-simulated thermal-history paths are obtained. Information on the detailed heat history modeling is presented in Table S1.

The thermal-history simulation results show that the Greater Khingan Mountains experienced three stages of cooling and heating, possibly related to uplift-induced exhumation and regional heating (Fig. 4). The first stage is expressed as rapid cooling between130 and 94 Ma with a temperature drop from about 120°C to about 60°C and a cooling rate of about 3°C/Ma. Using the assumed geothermal gradient, this cooling rate translates to an average erosion rate of 0.08 mm/a and a total exhumation of approximately 1 km. The second stage of rapid cooling occurred during 45–0 Ma when the temperature dropped from 105°C to 36°C at a rate of about 7°C/Ma. The results correspond to an exhumation rate of 0.19 mm/a and a total exhumation of approximately 1.8 km. The third stage is expressed by a heating event from 64 Ma to 45 Ma when the temperature increased from about 60°C to about 110°C. From the above modeling results, the total exhumation of the central Greater Khingan region has been about 3 km since ca. 130 Ma.

Figure. 4

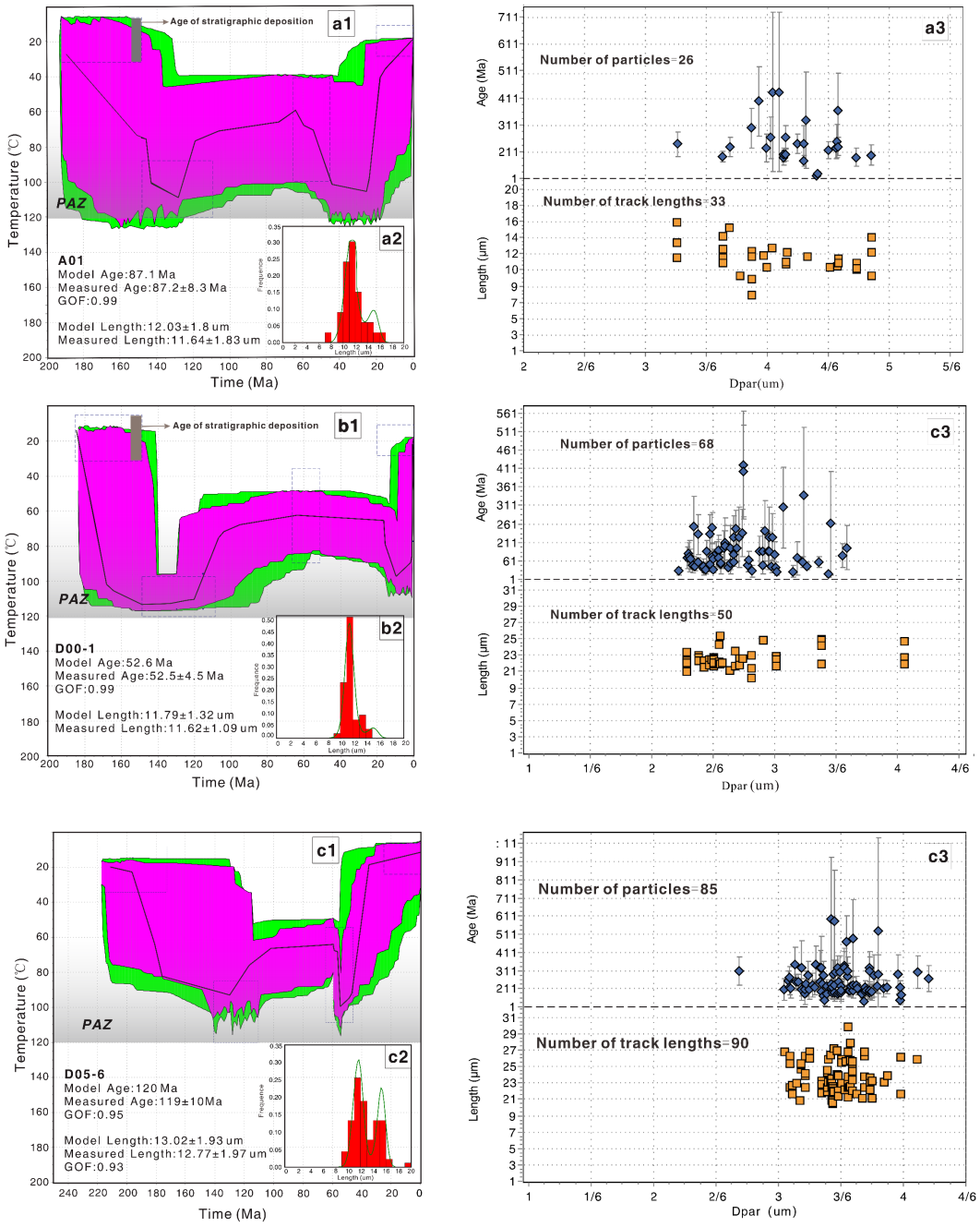
a1
Age of stratigraphic deposition
PAZ
a2
A01
Model Age:87.1 Ma
Measured Age:87.2±8.3 Ma
GOF:0.99
Model Length:12.03±1.8 um
Measured Length:11.64±1.83 um
Temperature (℃)
Time (Ma)
a3
Number of particles=26
Number of track lengths=33
Age (Ma)
Length (μm)
Dpar(um)
b1
Age of stratigraphic deposition
PAZ
b2
D00-1
Model Age:52.6 Ma
Measured Age:52.5±4.5 Ma
GOF:0.99
Model Length:11.79±1.32 um
Measured Length:11.62±1.09 um
Temperature (℃)
Time (Ma)
c3
Number of particles=68
Number of track lengths=50
Age (Ma)
Length (μm)
Dpar (um)
c1
PAZ
c2
D05-6
Model Age:120 Ma
Measured Age:119±10Ma
GOF:0.95
Model Length:13.02±1.93 um
Measured Length:12.77±1.97 um
GOF:0.93
Temperature (℃)
Time (Ma)
c3
Number of particles=85
Number of track lengths=90
Age (Ma)
Length (μm)
Dpar (um)

Figure 4. Simulation of the relationship between sample time temperature path (a1, b1, c1), length distribution (a2, b2, c2) and D_{par} value and sample single particle age and confining length (a3, b3, c3). In the T-T diagram, the black line is the best simulation curve, the pink area corresponds to the good fitting range (GOF > 0.5), and the green area corresponds to the acceptable fitting range (GOF = 0.05–0.5).

4.3 Three-dimensional Numerical Simulation

To verify the reliability of the thermal history simulation of uplift and exhumation events from the middle Early Cretaceous to the middle Late Cretaceous (130–94 Ma), we further tested our thermal-history results using Pecube 3D numerical simulations. The two tested samples (D05-6 and D08-6) were taken as the simulation objects, and the area near the location of the sample was selected as the simulation operation area (0.25° × 0.25°) (Fig. 1c). The resolution of each terrain model was 30 m, which is sufficient to distinguish the difference of the terrain data from the upper part of the terrain model; for the lower boundary of the model, the simulated crustal thickness was 40 km (Gao, 2014). In each simulation, we set 20 iterations, 600 iterations each time, and the resampling rate was fixed at 570 times (90%).

To find the exhumation event in the study area from the Early Cretaceous to the middle Late Cretaceous revealed by the thermal history simulation, two models were set up to explore the starting point and ending point of this exhumation event. Specific construction scenarios are presented in Table 4. For each stripping event, the terrain relief (R) was set to $R = 1$ and $R = 0.5{:}1.5$ for the simulation. $R = 1$ indicates that the topographic relief is stable in the simulated geological period; $R = 0.5{:}1.5$ indicates that an elastic interval is given to the topographic relief, so that the topographic relief changes with time in the process of geological evolution. The thermodynamic and geophysical parameters used in the model are shown in Table 3. The results in Table 4 represent the best model results obtained by multiple parameter optimization, and the results of the best model (presented in bold in Table 4) were selected as the final result.

Based on the dispersion degree of the misfit value and kernel function probability distribution curve, the simulation results of the steady-state scenario ($R = 1$) in the two models were better, and the constraints on stripping rate were more accurate (Figs. 6 and 7). Therefore, the steady-state topographic relief ($R = 1$) scenes in the stripping start point model and stripping end point model were considered to be more consistent with the geomorphic evolution of the study area.

The simulation results showed that in the two defined terrain models, the cooling history revealed by the inversion results was well constrained. Although the predicted age obtained by the two terrain models was generally consistent with the measured age of the data (Fig. 5), the convergence of the scatter diagram obtained by the inversion simulation results was significantly different (Figs. 6

and 7).

Table 3. Pecube thermodynamic and geophysical parameters.

Thermokinetic parameters	Numerical value	Reference	C
Crustal thickness	40 km	Gao et al., 2014	C
Sea level temperature	25°C	Bermudez et al., 2011	A
Thermal diffusion coefficient	25 km/Myr	Braun et al., 2012	Y
Atmospheric temperature gradient	6°C/km	Naito et al., 2006	P
Crustal heat generation rate	0°C/Myr	Braun et al., 2012	P

Table 4. List of Pecube model simulation parameters in different scenarios.

Geological period	Scene	Parameter range	Tagging	Optimal solution	Misfit
Early Cretaceous middle Late Cretaceous (starting point of exhumation)	Steady terrain (R = 1)	T1: 132 Ma T2: 93–132 Ma T3: 93 Ma	Transition time	T2: 128.72 Ma	**0.76**
		E1: 0:0.05 km/Myr E2: 0:0.15 km/Myr	Exhumation rate	E1: 0.034 km/Myr E2: 0.147 km/Myr	
		T: 700–900°C	Substrate temperature	T: 889.3°C	
	Dynamic terrain (R: 0.5–1.5)	T1: 132 Ma T2: 93–132 Ma T3: 93 Ma	Transition time	T2: 125.6 Ma	
		E1: 0–0.05 km/Myr E2: 0–0.15 km/Myr	Exhumation rate	E1: 0.02 km/Myr E2: 0.12 km/Myr	
		T: 700–900°C	Substrate temperature	T: 898.3°C	

Geological period	Scene	Parameter range	Tagging	Optimal solution	Misfit
		R1: 0.5–1.5 R2: 0.5–1.5	Topographic relief	R1: 0.8 R2: 1.3	

continued

Geological period	Scene	Parameter range	Tagging	Optimal solution	Misfit
Early Cretaceous middle Late Cretaceous (end point of exhumation)	Steady terrain (R = 1)	T1: 132Ma T2: 90–132Ma T3: 90Ma	Transition time	T2: 98 Ma	**0.76**
		E1: 0–0.15 km/Myr E2: 0–0.05 km/Myr	Exhumation rate	E1: 0.137 km/Myr E2: 0.045 km/Myr	
		T: 700-900°C	Substrate temperature	T: 878.4°C	
	Dynamic terrain (R: 0.5–1.5)	T1: 132 Ma T2: 90–132 Ma T3: 90 Ma	Transition time	T2: 95.1 Ma	
		E1: 0–0.15 km/Myr E2: 0–0.05 km/Myr	Exhumation rate	E1: 0.07 km/Myr E2: 0.04 km/Myr	
		T: 700–900°C	Substrate temperature	T: 853.6°C	
		R1: 0.5–1.5 R2: 0.5–1.5	Topographic relief	R1: 0.74 R2: 0.87	

Note: The corresponding result of the bold misfit value is the optimal solution.

Figure. 5

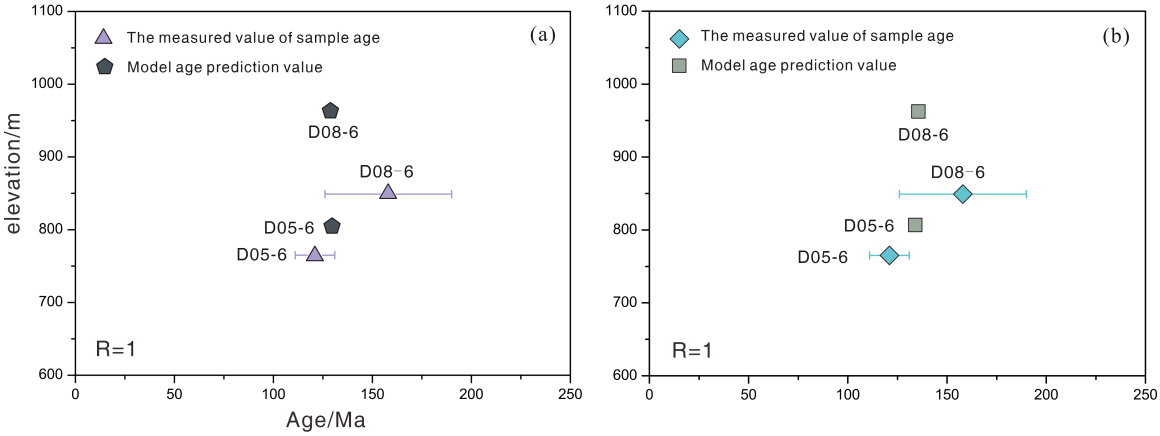

Figure 5. Comparison of measured and predicted apatite fission-track (AFT) values in different scenarios. (a) Steady state terrain starting point model ($R = 1$). (b) Steady state terrain end point model ($R = 1$).

For the Early Cretaceous–middle Late Cretaceous starting point model, in the simulation scenario of stable terrain (Table 4; Fig. 6), the two-dimensional scatter diagram showed great convergence. The start time of the stripping event was also well constrained, and the maximum probability occurred at ~129 Ma (Fig. 6a). The optimum stripping rate was 0.034 km/Myr between 132 and 129 Ma (Fig. 6c), and 0.147 km/Myr between 129 and 93 Ma (Fig. 6d). The stripping rate increased significantly after the conversion time (Fig. 6c, d). The base temperature reached the maximum probability at 889.3°C (equivalent to the ground temperature gradient of 22.2°C/km) (Fig. 6a). The kernel function probability curves of stripping rate and substrate temperature parameters exhibited the distribution characteristics of a single peak (high probability value) with great convergence, and the peak was obvious (Fig. 6a, b). The distribution state of the kernel function probability curve of the conversion time parameter was also relatively set (Fig. 6a). The minimum misfit value of the model was 0.76. The low misfit value had strong correlation and good convergence with the peak value (high probability value) of each parameter. See the Supplementary drawing for the dynamic terrain model (Figs. S3–S5).

Figure. 6

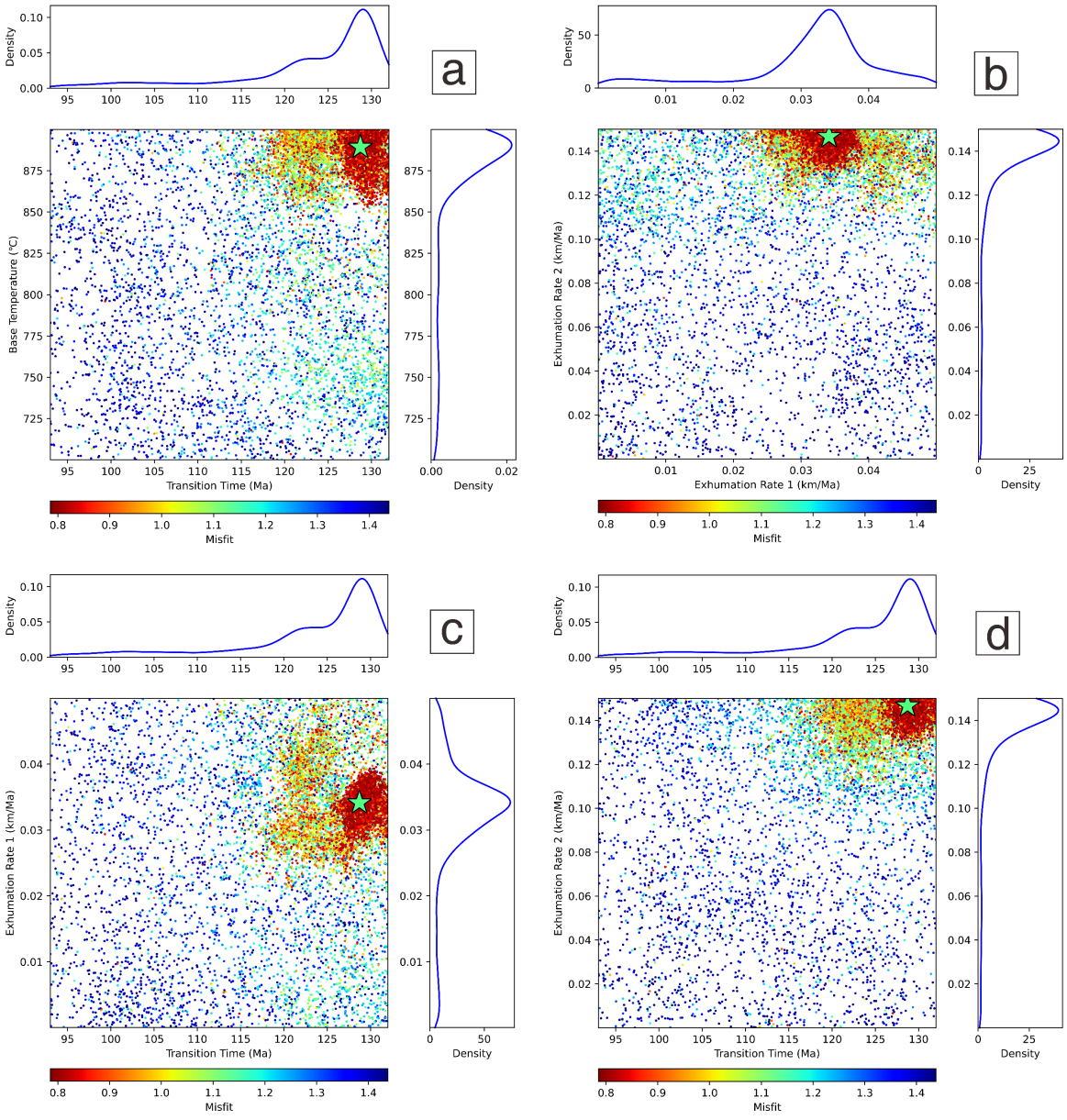

Figure 6. Pecube inversion results based on apatite fission-track (AFT) steady-state topographic starting point model. The inversion results are projected onto the two-dimensional scatter diagram. (a) Scatter diagram of conversion time T2 and substrate temperature. (b) Scatter diagram of exfoliation rate E1 and E2.

(c) Scatter diagram of conversion time T2 and stripping rate E1. (d) Scatter diagram of conversion time T2 and stripping rate E2. The scatter color value represents the misfit error value. The upper and right blue curves are kernel function probability curves, and the probability increases upward and right. The green Pentagram represents the best fit value.

For the Early Cretaceous–middle Late Cretaceous termination point model, in the inversion results of steady-state terrain, the cooling history of two-stage evolution was well-constrained (Fig. 7). The end time constraint of rapid exhumation was very good, and the maximum probability occurred at 98 Ma (Fig. 7a). During the rapid stripping period of 132–98 Ma, the stripping rate reached 0.137 km/Myr (Fig. 7c), while after the end of the rapid stripping period, the model reflected that the stripping rate decreased to 0.045 km/Myr between 98 and 90 Ma (Fig. 7d). The base temperature with the maximum probability was 878.4°C (equivalent to the ground temperature gradient of 22°C/km) (Fig. 7a). The best misfit value was 0.76. The peak value of the kernel probability density distribution of the first stage stripping rate was obvious, and the kernel probability density distribution of other parameters also showed good convergence (Fig. 7). See the Supplementary Figures for the dynamic terrain model (Figs. S3–S5).

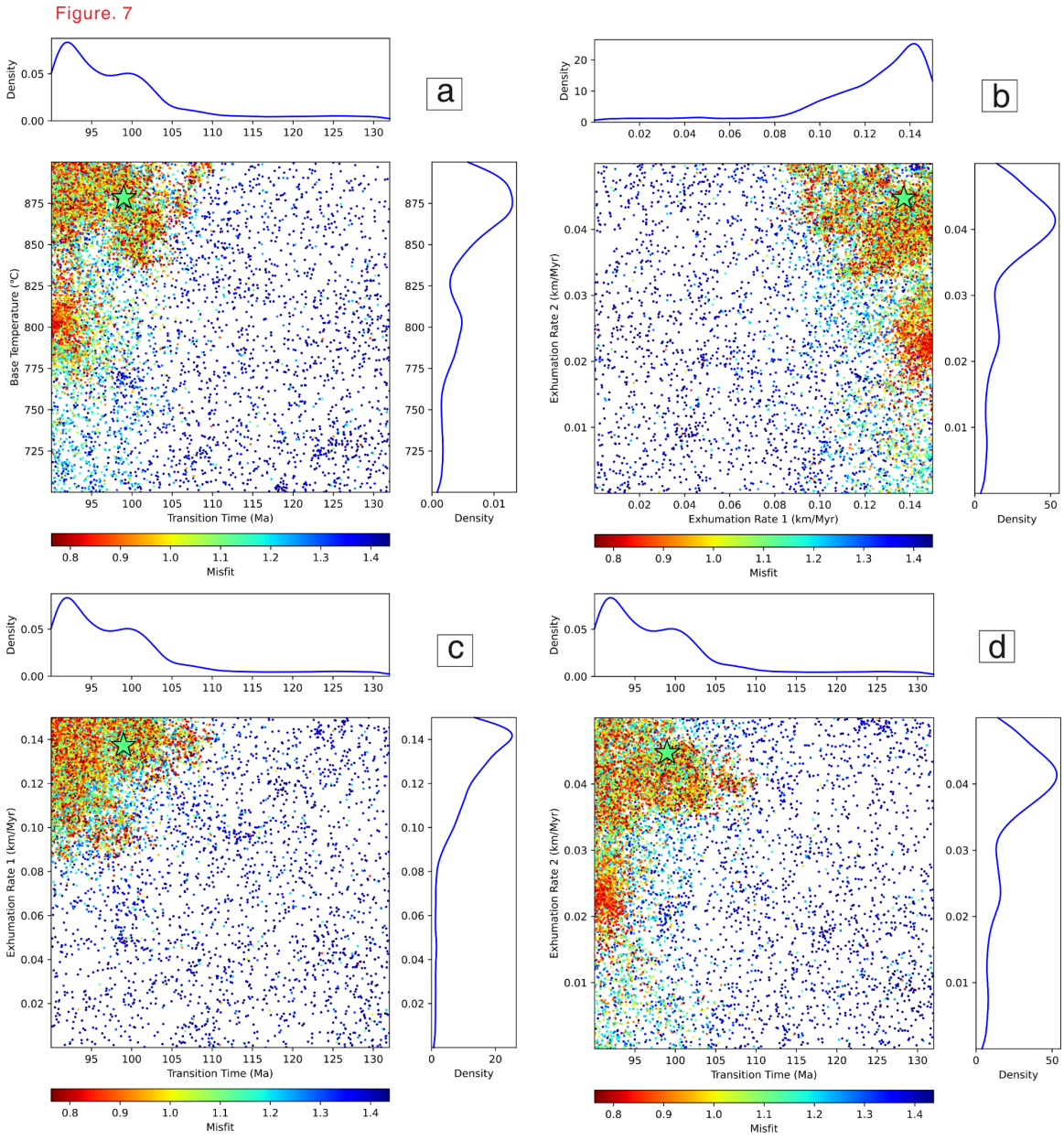

Figure 7. Pecube inversion results based on apatite fission-track (AFT) steady-state topographic endpoint model. The inversion results are projected onto the two-dimensional scatter diagram. (a) Scatter diagram of conversion time T2 and substrate temperature. (b) Scatter diagram of exfoliation rate E1 and E2. (c) Scatter diagram of conversion time T2 and stripping rate E1. (d) Scatter

diagram of conversion time T2 and stripping rate E2. The scatter color value represents the misfit error value. The upper and right blue curves are kernel function probability curves, and the probability increases upward and right. The green Pentagram represents the best fit value.

5 Discussion

The provenance of the sedimentary rock samples is relatively complex. The sampled Murui Formation was deposited in a thrust-induced basin (Li et al., 2015). Provenance analysis of sandstone samples from the Murui Formation indicates an active continental margin setting, specifically derived from thrust blocks next to the sample sites. The AFT cooling and heating events may have resulted from tectonic exhumation events in the Greater Khingan area since the Late Jurassic. The statistical results of the single-particle age of the five apatite samples in this sample showed that the peak particle age is concentrated in the late Mesozoic and Cenozoic eras (Fig. 8a). The apatite particles underwent annealing and track preservation during this period, indicating that the study area experienced intense exhumation during this period. The statistical results (Fig. 8b, details of the reference data are presented in Table S2) show that a strong thermal event occurred in the Greater Khingan Mountains before the Early Cretaceous, which resulted in the complete annealing and resetting of the older AFT ages, as indicated by the track lengths shorter than 16.3 ± 0.9 µm. The age-length distribution of the samples displays a "boomerang" pattern (Gleadow et al., 1986) that requires complex annealing events created by multiple tectonic events.

Figure. 8

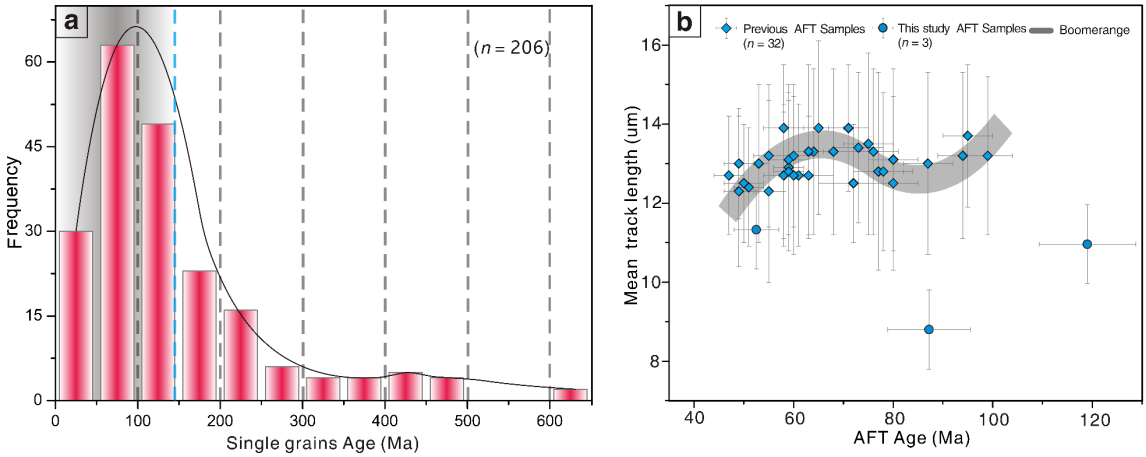

Figure 8. (a) The age distribution frequency of a single grain from five samples was studied ($n = 206$). (b) The age-length distribution map of the apatite fission-track (AFT) in the Greater Khingan Mountains area shows the "boomerang" model. Data from this study and previous data from Li et al. (2011), Wu et al. (2016), and Pang et al. (2020). AFT samples from this study are D05-6, D00-1,

and P1-11.

5.1 Comparison of Two Simulation Methods

The 2D HeFty thermal history simulation indicates that the starting point of this cooling event was 130 Ma and the ending point was 94 Ma. The cooling rate in the rapid cooling stage was 0.06 km/Myr (the ground temperature gradient is 30°C/km). The inversion results of the Pecube 3D model (steady-state terrain) show that the best conversion times are 129 Ma and 98 Ma, and the maximum probability values of the rapid stripping rate (E2) are 0.147 and 0.137 km/Myr (the ground temperature gradient is 22.2°C /km). There is a difference between the ages predicted by the forward modeling and the Pecube model as well as the estimated and measured altitude values, and there is also a difference in the cooling rate in the rapid cooling stage between the two simulation methods. These discrepancies may be related to the different calculation methods of the two simulation methods, and also the ground temperature gradient assumed by the HeFty 2D thermal history simulation is uniformly distributed, which may be different from reality. In contrast, we believe that the results of the 3D numerical simulation are more consistent with the real geomorphic evolution.

5.2 Episodic Exhumation Events

The results of the thermal history simulation show that the Greater Khingan area has experienced several thermal events since the Early Cretaceous: a cooling event in the Early Cretaceous-Late Cretaceous (130–94 Ma), a cooling event in the Eocene to the present (45–0 Ma) intervened by a regional heating event in the Paleocene-Eocene between 64 and 45 Ma. The tectonic implications of these thermal events are discussed below.

The cooling event between 130 and 94 Ma was determined based on samples from the Murui Formation, which consists of cobbles with sizes that vary cyclically in the stratigraphic sequence. An unconformity is present between the upper and lower section, which might have a tectonic origin. Sample D05-6 taken from the thrust hanging wall yielded the most apatite grains ($N = 85$) with a center age of 121 ± 10 Ma. This age may represent the tectonic activity of the thrust fault in the Early Cretaceous, which is consistent with the timing of thrusting in the area inferred by other researchers (Li et al., 2015). Except for sample P1-11, the center ages of the remaining samples were younger than or close to the stratigraphic ages of the samples (Fig. 3). The peak age of P1-11 was 155 ± 21 Ma, which is very close to the stratigraphic age of the sample. Combined with the peak-age decomposition results of other samples, the peak age between 41.9 ± 5.5 and 46.2 ± 4.3 Ma for sample P1 and the peak age between 159 ± 30 Ma and 108 ± 28 Ma for sample P2 (Table. 2) may indicate that a regional exhumation event occurred in the central Greater Khingan Mountains during this period, which coincides with a cooling stage indicated by our thermal history simulation results (Figs. 4 and S2). In addition, the track lengths of all samples less than the expected initial track length indicate that the samples have undergone partial annealing and thermal resetting. The U-Pb detrital

zircon dating of the Murui Formation yields an aging cluster at 147–146 Ma (Li et al., 2015), and the younger cooling ages inferred here from the same stratigraphic unit are consistent with the AFT cooling history being induced after the deposition of the sampled material.

The AFT study of the Mohe Basin (Fig. 1b) in the northern part of the Greater Khingan Mountains also revealed a 120–90 Ma exhumation event (Wu et al., 2016), which coincides with the first phase of the cooling event deduced from this study (Fig. 9a). This correlation implies that the same cooling event and associated exhumation occurred across the Greater Khingan Mountains as a whole. Volcanism in Northeast China mainly occurred between 133 Ma and 88 Ma (Xu et al., 2013). Highly differentiated Early Cretaceous I- and A-type granitoids and bimodal volcanic rocks also occur across the Greater Khingan Mountains area (Fig. 9d) (Jahn et al., 2000; Jahn et al., 2001; Wei et al., 2002; Liu et al., 2005; Dong et al., 2014; Li et al., 2015; Sun et al., 2017). This phase of igneous activity was closely associated with polymetallic mineralization and coal-bearing fault-bounded basin formation in the area (Yang et al., 2015; Duan et al., 2018). It was also accompanied by an extension (Xu et al., 2013) expressed as the Greater Khingan Mountains metamorphic core complexes developed between 120 Ma and 130 Ma (Miao et al., 2004; Zhao et al., 2007; Zeng et al., 2011; Yang et al., 2014), and the formation of the extensional Songliao Basin at 127 $\pm$ 2 Ma (Fig. 1b) (Wang et al., 2011). In addition, seismic tomography across the Greater Khingan Mountains indicates that delamination occurred in the lower crust (Xiong et al., 2015).

Figure. 9

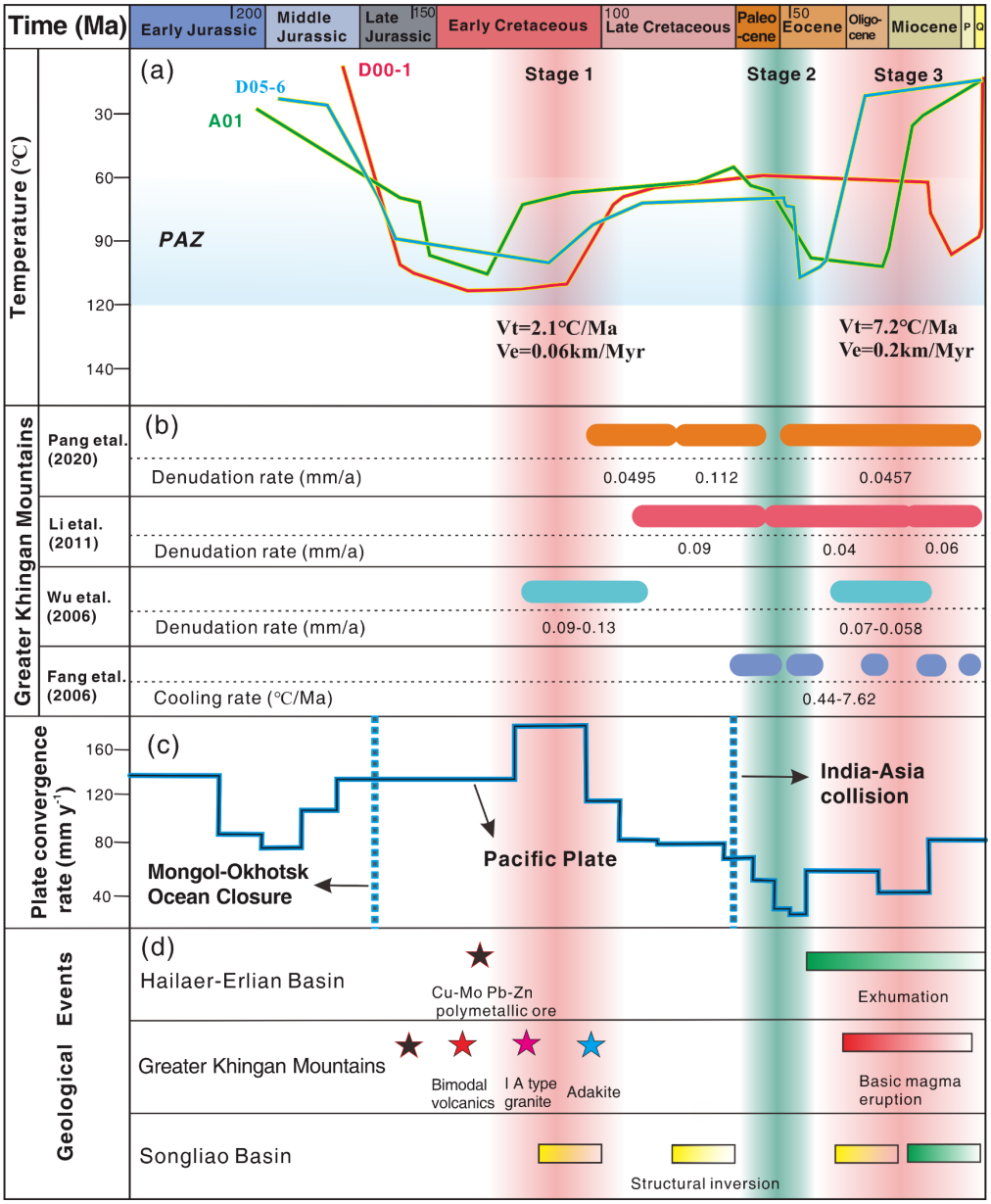

Figure 9. (a) Summary of thermal history simulation results. (b) The exudation process and exudation rate of the Greater Khingan Mountains (data from Fang et al., 2005; Li et al., 2011; Wu et al., 2016; Pang et al., 2020). (c) Mongolian Okhotsk Ocean closure time (according to Kravchinsky et al., 2002; Cogné et al., 2005; Tomurtogoo et al., 2005; Metelkin et al., 2007; Zhang et al., 2011)

and Pacific plate convergence rate (data from Northrup and Royden, 1995; Barbarand et al., 2003). Age data of the India-Asia collision from Donskaya et al. (2013) and Meng et al. (2018). (d) Major tectonic events (volcanic activity data from Li et al., 2020 and Xu et al., 2020). Tectonic reversal data from Cheng et al. (2018). I- and A-type granites and bimodal volcanic rocks from Jahn et al. (2000), Jahn et al. (2001), Wei et al. (2002), Liu et al. (2005), Dong et al. (2014), Li et al. (2015), and Sun et al. (2017). Cu-Mo, Pb-Zn polymetallic ore data from Yang et al. (2015), Duan et al. (2018), and Tang et al. (2018).

The Hailar-Erlian Basins (Fig. 1b) in the Early Cretaceous experienced NNW-SSE extension on the south side of the Mongolia-Okhotsk Ocean suture zone (Liu et al., 2009; Yang et al., 2015; Zhang et al., 2017). During the same period, the Songliao Basin continued to develop in an extensional environment (Liu et al., 1993). The rapid exhumation of the Greater Khingan Mountains and the rapid subsidence of the Songliao Basin and Hailar Basin suggest that the mountain exhumation and basin formation were coupled as a result of the regional extension.

The reheating event between 66 and 40 Ma (Figs. 4 and S2) may have been induced by combined burial and rising heat flux (Pang et al., 2020). Pang et al. (2020) argue that dewatering of subducted slabs of the Paleo-Asian Ocean plate may have induced partial melting and asthenospheric upwelling below Northeast China. During the Cenozoic, the Greater Khingan Mountains were affected by widely occurring volcanism (Li et al., 2020; Xu et al., 2020) (Fig. 9d), which may have contributed to the regional heating event shown in the simulation results. We have found that similar age peaks between 66 and 40 Ma exist in Northeast Asia (Fig. 10, the details of the reference data are provided in Table S3), which indicates that the event was regional in scale. During this period, the Pacific plate changed its motion from NNW to NW in the direction of subduction (Fig. 12) and the plate convergence rate reached a low-velocity peak (Fig. 9c) (Engebretson, 1985; Grebennikov et al., 2016). The reduced Pacific plate convergence rate and the onset of the India–Asia collision created a condition between 60 and 55 Ma that favored the reheating of the Greater Khingan Mountains (Donskaya et al., 2013; Meng et al., 2018).

The thermal history simulation results show that the second rapid exhumation event in the Greater Khingan Mountains occurred in the period 30–15 Ma (Figs. 4 and S3). The existing fission track studies all indicate that a rapid exhumation event occurred since ca. 30 Ma (Fig. 9b) (Fang et al., 2005; Li et al., 2011; Wu et al., 2016; Pang et al., 2020). Northeast Asia was under extension during this period (Gaina et al., 2002; Suo et al., 2020).

Songliao Basin experienced structural inversion at ca. 37–34 Ma and ca. 25 Ma, which caused the exhumation of the basin (Fig. 9d) that started in the east and migrated westward (Cheng et al., 2018). The exhumation rate of the basin has been correlated with the increasing subduction rate of the Pacific plate (Xiang et al., 2007; Cheng et al., 2020; Wang et al., 2020a). The thermal history of the Weijing pluton near the Hailar Basin and the southern Songliao Basin implies

that the basin exhumation event corresponds to the cooling event in the Greater Khingan Mountains at ca. 30 Ma (Fig. 9d) (Nie et al., 2018; Cheng et al., 2020; Wang et al., 2020a). This in turn supports the notion that the exhumation of the Greater Khingan Mountains and the Hailar Basin and Songliao Basin were coupled in the Late Cenozoic (Wu et al., 2011; Li et al., 2011).

Figure. 10

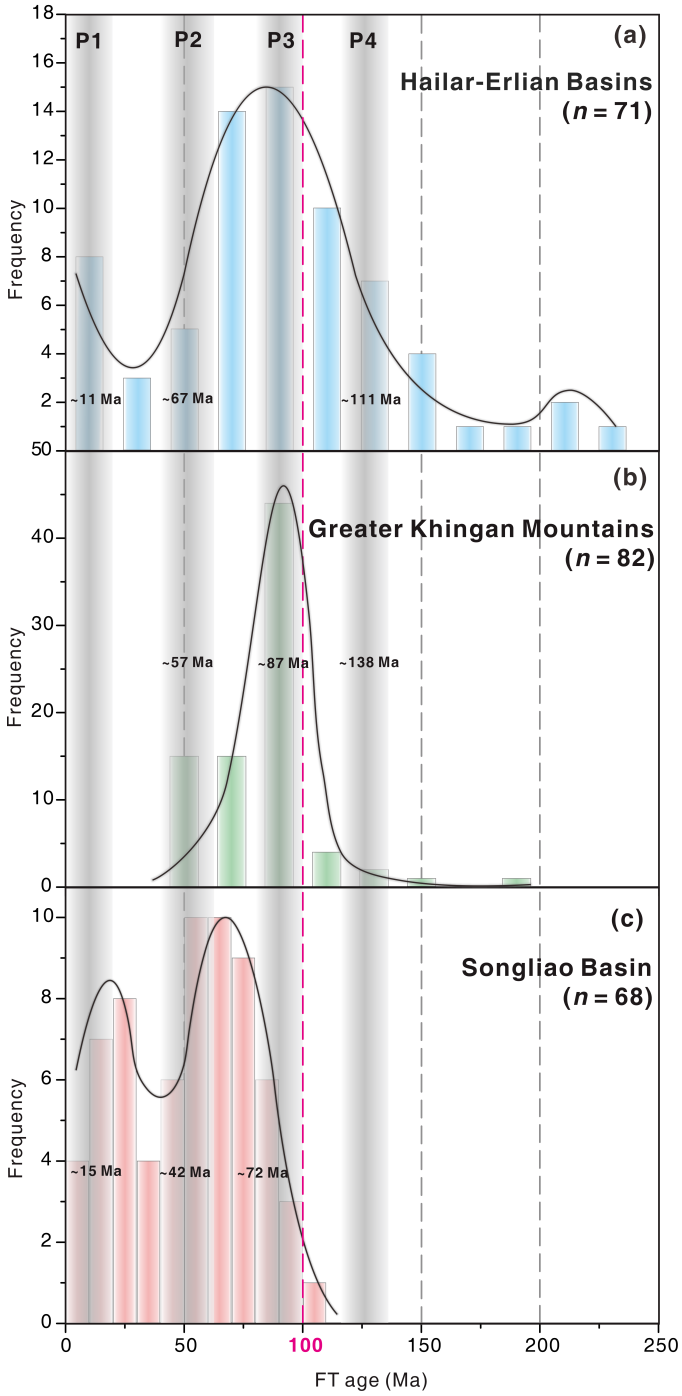
P1
P2
P3
P4
(a)
Hailar-Erlian Basins
(n = 71)
~11 Ma
~67 Ma
~111 Ma
(b)
Greater Khingan Mountains
(n = 82)
~57 Ma
~87 Ma
~138 Ma
(c)
Songliao Basin
(n = 68)
~15 Ma
~42 Ma
~72 Ma
Frequency
FT age (Ma)
0
50
100
150
200
250

Figure 10. Fission-track age frequency map (FT, AFT). (a) Hailar-Erlian Basins fission-track age frequency data from Zhao et al. (1998), Cui et al. (2007), Cui et al. (2011), Cui and Ren (2011), Cui et al. (2015), Zuo et al. (2015), Zuo et al. (2016), Nie et al. (2018) and Guo et al. (2018). (b) Greater Khingan Mountains fission-track age frequency data from Li et al. (2011), Wu et al. (2016), Pang et al. (2020) and this study. (c) Songliao Basin fission-track age frequency map data from Xiang et al. (2007), Cheng et al. (2020), Wang et al. (2020a), and Wang et al. (2020b).

5.3 Regional Tectonic Implications

Inferred exhumation events in the Greater Khingan Mountains are summarized in Fig. 9. The figure shows that the Greater Khingan Mountains have experienced multiple stages of exhumation events since the Early Cretaceous, and the exhumation rate has been in the range of 0.03–0.19 mm/a. The Greater Khingan Mountains and Hailar-Erlian Basins have similar clustered AFT cooling ages between 160 and 100 Ma (peak age 4 in Fig. 10). Although the Greater Khingan Mountains experienced a cooling event between 130 and 95 Ma, this event is absent in the Songliao Basin. A magnetotelluric study of the tectonic boundary zone between the Greater Khingan Mountains and the Hailar and Songliao basins revealed that the eastern margin of the Hailar Basin belongs to the Xing'an terrane, and that the contact between the western margin of the Songliao Basin and the easternmost Greater Khingan Mountains is a thrust wedge system (Xiong et al., 2015). The Hailar-Erlian Basins were a group of extensional basins formed in the Early Cretaceous, and their development was associated with the tectonic history of the Greater Khingan Mountains (Liu et al., 2009; Yang et al., 2015; Zhang et al., 2017).

The AFT cooling ages in the Greater Khingan Mountains have been decreasing from west to east since the Early Cretaceous (Li et al., 2011). The peak U-Pb zircon ages of magmatism from the Hailar Basin, through the Greater Khingan Mountains, and reaching the Songliao Basin show that there is a decreasing age trend (Zhang et al., 2011; Sorokin et al., 2014). However, there is no obvious intermittent period of magmatism in the Greater Khingan Mountains area during this period, and there is an obvious intermittent period of magmatic activity in the eastern Songliao Basin (Wang et al., 2006; Tang et al., 2018; Wang et al., 2018). The above evidence indicates that regional volcanic activity and exhumation events since the Early Cretaceous first began in the northwest of the Greater Khingan Mountains and then transitioned to the southeast. It also implies that the Greater Khingan Mountains and the Songliao Basin to the east belong to different tectonic domains. We believe that the spatial distribution characteristics of the magmatic zircon and AFT ages of the Greater Khingan Mountains in the Early Cretaceous are more likely to be related to extensional tectonics after the closure of the Mongolia-Okhotsk Ocean.

The AFT ages of the Greater Khingan Mountains, Hailar-Erlian Basins, and Songliao Basin show three sets of similar peak ages (age peaks 2 and 3 in Fig. 10) in the range of 100–42 Ma. In the Late Jurassic-earliest Cretaceous, magmatism

and porphyry Cu-Mo and Pb-Zn polymetallic deposits were mainly distributed in the west of Songliao Basin (Fig. 9d) (Yang et al., 2015; Duan et al., 2018; Tang et al., 2018). During the middle and late Early Cretaceous, volcanism occurred widely throughout Northeast China (Wu et al., 2005; Sun et al., 2013; Tang et al., 2018). The basins on both sides of the Greater Khingan Mountains experienced tectonic inversion in the latest Cretaceous and the Late Paleogene. This indicates that the basin-mountain system composed of the Greater Khingan Mountains and the basins on both sides may be affected by the same tectonic stress field. The spatiotemporal distribution of the AFT ages in the Songliao Basin displays a trend of increasing ages to the west (Xiang et al., 2007).

Based on the previous discussion, we interpret that the Greater Khingan Mountains developed by extensional tectonics between ca. 130 and 95 Ma. The Mongolian-Okhotsk Ocean began to close no earlier than the Middle Jurassic and ended its closure process in the Early Cretaceous (Kravchinsky et al., 2002; Sorokin et al., 2004; Galbraith & Laslett, 1993; Tomurtogoo et al., 2005; Metelkin et al., 2007; Zhang et al., 2011; Sorokin et al., 2020). Adakite in the Greater Khingan Mountains emplaced during this period may have resulted from crustal thickening and mantle-lithospheric delamination (Fig. 9d) (Wu et al., 2011; Zhang et al., 2019). At this time, the Izawa-Nasaki plate, which constitutes the paleo-Pacific plate, subducted in the NNE direction at a high speed below the northeast Asian continent. At this time, motion and subduction of the Pacific plate were not the main driving force for the regional expansion of the Greater Khingan Mountains. Rather, the gravitational collapse of the orogenic belt in the study area created by the closure of the Mongol-Okhotsk Ocean induced regional extension that in turn created the Greater Khingan Mountains and Hailar-Erlian Basins. In addition, the trench retreat of the western Pacific subduction zone in the late Early Cretaceous period (Fig. 12a) (Tang et al., 2018) may have provided a favorable condition for regional expansion.

Figure. 11

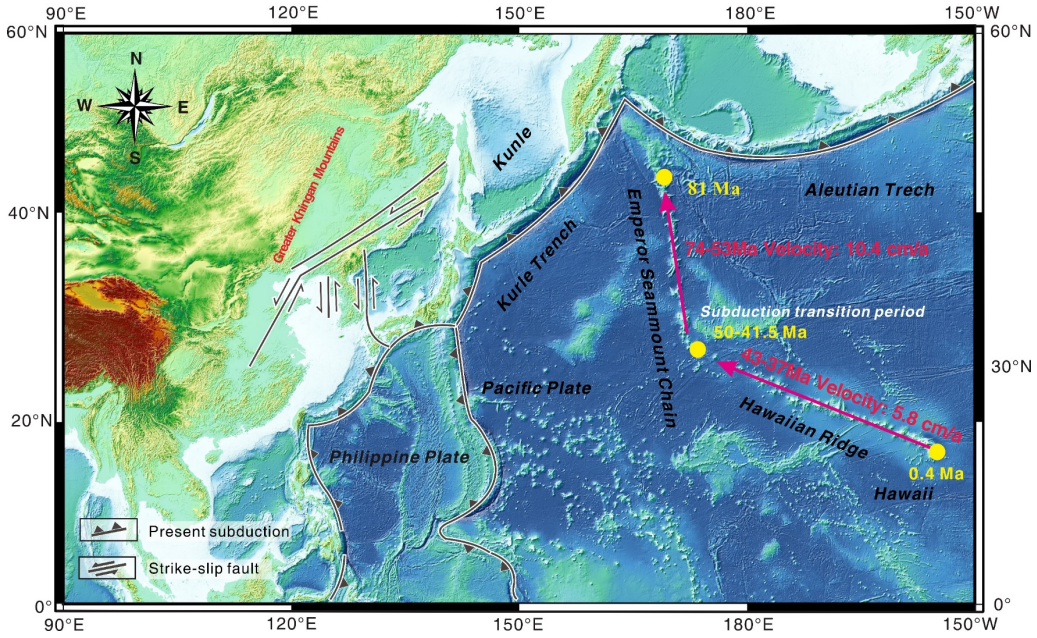

Figure 11. Hawaii-Emperor Islands map showing the main changes in the direction and time of the Pacific plate movement, modified after Sharp and Clague (2006), Cheng et al. (2018), and Cheng et al. (2020).

Since ca. 30 Ma, the Greater Khingan area has remained under extension. The subduction direction of the Pacific plate has undergone transition at ca. 10 Ma during the period between 50 and 42 Ma. The relative subduction rate of the Eurasian plate has increased in general since the Eocene (Fig. 11) (Northrup and Royden, 1995). This process controlled back-arc expansion and right-lateral strike-slip faulting in Northeast Asia (Fig. 12b).

Figure. 12

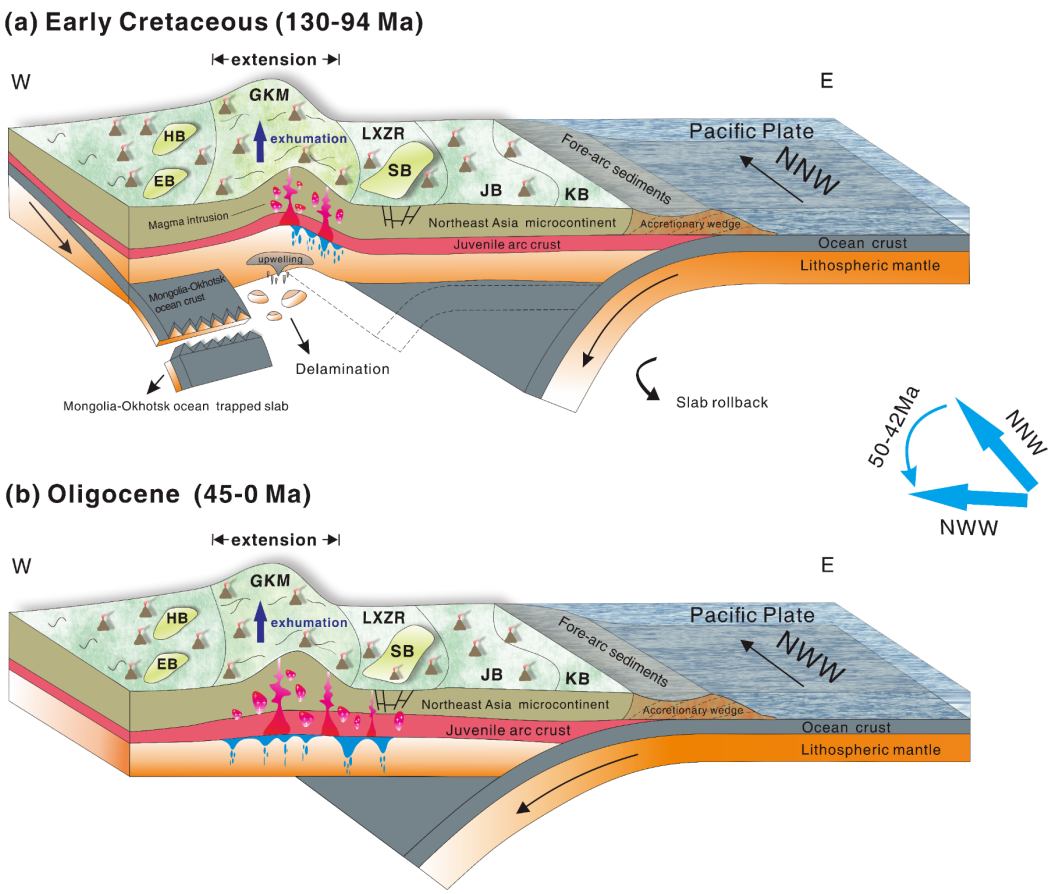

Figure 12. Evolutionary block diagrams that show two stages of tectonic evolution in the Greater Khingan Mountains region since the Early Cretaceous. (a) The first stage is expressed by the Early Cretaceous (130–95 Ma) post-orogenic extension. (b) The second stage is expressed by the Eocene (30–0 Ma) post-arc-magmatism extension. Adapted from Tang et al. (2018) and Cheng et al. (2020).

6 Conclusions

AFT dating and a synthesis of the existing geologic information led us to make the following conclusions:

1. The AFT ages and thermal history simulation results reveal three cooling events between 130–94 Ma and 45–0 Ma and one reheating event (64–45 Ma) in the Greater Khingan Mountains since the Early Cretaceous. The total amount of exhumation has been 3 km since ca. 130 Ma.

2. The AFT data in the study area were used to set different simulation scenarios for 3D thermal dynamics modeling to verify the stripping starting point and stripping end point of the cooling stripping event from the Early Cretaceous to the middle Late Cretaceous (130–94 Ma) in the central Great Khingan Mountains revealed by the 2D thermal history simulation. The inversion results of the three-dimensional model (steady-state terrain) show that the best conversion times are 128.72 Ma and 98 Ma. The maximum probability values of the rapid stripping rate (E2) are 0.147 and 0.137 km/Myr (the ground temperature gradient is 22.2°C/km).

3. The Greater Khingan Mountains and Hailar-Erlian Basins share similar AFT peak ages between 160 Ma and 100 Ma, while the Songliao Basin does not have such a correlation. We suggest that the Greater Khingan Mountains and Hailar-Erlian Basins have a common tectonic evolution history during this period. From 100 Ma to 42 Ma, the Greater Khingan Mountains, Hailar-Erlian Basins, and Songliao Basin share similar AFT peak ages, which suggests that the three tectonic domains were integrated into a unified tectonic system.

4. We suggest that the gravitational collapse of an orogenic belt in Northeast China induced by the closure of the Okhotsk Ocean was the main cause of the first cooling event in the region between 130 and 94 Ma. Subsequent cooling and reheating in the region have been controlled by the interaction between the Pacific plate and Northeast Asia since about 100 Ma.

Acknowledgments

We thank the personnel of the Key Laboratory of Western Gansu Mineral Resources of Lanzhou University and the Public Technical Service Center of the Lanzhou Oil and Gas Resource Center of the Chinese Academy of Sciences for their help with apatite fission-track (AFT) analysis. We also give thanks to Professor An Yin of the University of California, Los Angeles, for his suggestions on revising the article. This work was supported by the National Nature Science Foundation of China (grant number 41872234) and the Opening Foundation of Key Laboratory of Mineral Resources Evaluation in Northeast Asia, Ministry of Natural Resources (grant number DBY-ZZ-18-08).

Conflict of Interest

The authors declare no conflicts of interest relevant to this study.

Data Availability Statement

This research data is stored on https://zenodo.org/deposit/6526169. The thermal history simulation software used in this study is available via Ketcham., et al 2009; https://doi.org/10.1016/j.epsl.2009.05.015 for, Pecube numerical simulation program by Braun, J, 2003; https://doi.org/10.1016/S0098-3004 (03), 00052-9.

References

Barbarand, J., Carter, A., Wood, I., & Hurford, T. (2003). Compositional and structural control of fission-track annealing in apatite. *Chemical Geology*, *198*, 107-137. https://doi.org/10.1016/s0009-2541(02)00424-2

Braun, J. (2003). Pecube: a new finite-element code to solve the 3D heat transport equation including the effects of a time-varying, finite amplitude surface topography. *Computers & Geosciences, 29,* 787-794.

https://doi.org/10.1016/S0098-3004(03)00052-9

Braun J., Peter V. D. B., Pierre V., Xavier R., Frédéric H., Christoph G., Vivi P., Claire P., Thibaud S. L., & Cécile P. (2012). Quantifying rates of landscape evolution and tectonic processes by thermochronology and numerical modeling of crustal heat transport using PECUBE. *Tectonophysics, 524-525,* 1-28.

Chen, Y.J., Zhang, C., Wang, P., Pirajno, F., & Li, N. (2017). The Mo deposits of Northeast China: A powerful indicator of tectonic settings and associated evolutionary trends. *Ore Geology Reviews, 81,* 602-640. https://doi.org/10.1016/j.oregeorev.2016.04.017

Cheng, Y.H., Wang, S.Y., Li, Y., Ao, C., Li, Y.F., Li, J.G., Li, H.L., & Zhang, T.F. (2018). Late Cretaceous–Cenozoic thermochronology in the southern Songliao Basin, NE China: New insights from apatite and zircon fission track analysis. *Journal of Asian Earth Sciences, 160,* 95-106. https://doi.org/10.1016/j.jseaes.2018.04.015

Cheng, Y.H., Wang, S.Y., Zhang, T.F., Teng, X.M., Ao, C., Jin, R.S., & Li, H.L. (2020). Regional sandstone-type uranium mineralization rooted in Oligo–Miocene tectonic inversion in the Songliao Basin, NE China. *Gondwana Research, 88,* 88-105. https://doi.org/10.1016/j.gr.2020.08.002

Cogné, J.P., Kravchinsky, V.A., Halim, N., & Hankard, F. (2005). Late Jurassic-Early Cretaceous closure of the Mongol-Okhotsk Ocean demonstrated by new Mesozoic palaeomagnetic results from the Trans-Baïkal area (SE Siberia). *Geophysical Journal International, 163,* 813-832. https://doi.org/10.1111/j.1365-246X.2005.02782.x.

Cui, J.P., & Ren, Z.L., 2011, Thermal evolution history of Wuerxun Sag in Hailaer Basin, Inner Mongolia [in Chinese with English abstract]. *Geoscience, 25,* 668-674.

Cui, J.P., Ren, Z.L., & Chen, Y.L.(2011). Study on the relationship between thermal evolution history and oil and gas in Beier Sag of Hailaer Basin [in Chinese with English abstract]. *Acta Sedimentologica Sinica, 29,* 388-394.

Cui, J.P., Ren, Z.L., Li, J.X., Yin, L.L., & Wang, W.Q. (2015). Restoration of thermal evolution history of Hulunhu Depression in Hailaer Basin [in Chinese with English abstract]. *Oil & Gas Geology, 36,* 35-42.

Cui, J.P., Ren, Z.L., & Xiao, H. (2007). Relationship between thermal evolution history and oil and gas in Huhehu Sag of Hailaer Basin [in Chinese with English

abstract]. *Geology In China, 34,* 522-527.

Donelick, R.A. (2005). Apatite Fission-Track Analysis. *Reviews in Mineralogy and Geochemistry, 58,* 49-94. https://doi.org/10.2138/rmg.2005.58.3

Dong, Y., Ge, W.C., Yang, H., Zhao, G.C., Wang, Q.H., Zhang, Y.L., & Su, L. (2014). Geochronology and geochemistry of Early Cretaceous volcanic rocks from the Baiyingaolao Formation in the central Great Xing'an Range, NE China, and its tectonic implications. *Lithos, 205,* 168-184. https://doi.org/10.1016/j.lithos.2014.07.004

Donskaya, T.V., Gladkochub, D.P., Mazukabzov, A.M., & Ivanov, A.V. (2013). Late Paleozoic – Mesozoic subduction-related magmatism at the southern margin of the Siberian continent and the 150 million-year history of the Mongol-Okhotsk Ocean. *Journal of Asian Earth Sciences, 62,* 79-97. https://doi.org/10.1016/j.jseaes.2012.07.023

Duan, P.X., Liu, C., Mo, X.X., Deng, J.F., Qin, J.H., Zhang, Y., & Tian, S.P. (2018). Discriminating characters of ore-forming intrusions in the super-large Chalukou porphyry Mo deposit, NE China. *Geoscience Frontiers, 9,* 1417-1431. https://doi.org/10.1016/j.gsf.2018.04.003

Eizenhöfer, P.R., Zhao, G., Zhang, J., & Sun, M. (2014). Final closure of the Paleo-Asian Ocean along the Solonker Suture Zone: Constraints from geochronological and geochemical data of Permian volcanic and sedimentary rocks. *Tectonics, 33,* 441-463. https://doi.org/10.1002/2013TC003357

Engebretson, D. (1985). Relative Motions Between Oceanic and Continental Plates in the Pacific Basin. *Geol.soc.amer.spec.pap, 206,* 1-60.

Fang, S., Liu, Z.J., & Guo, W. (2005). Coupling study of Cenozoic thermal structure between Songliao Basin and Daxing 'anling [in Chinese with English abstract]. *Nuclear Techniques, 28,* 717-721.

Gaina, C., Roest, W.R., & Müller, R.D. (2002). Late Cretaceous–Cenozoic deformation of northeast Asia. *Earth and Planetary Science Letters, 197,* 273-286. https://doi.org/10.1016/S0012-821X(02)00499-5

Galbraith, R.F., & Laslett, G.M. (1993). Statistical models for mixed fission track ages. *Nuclear Tracks and Radiation Measurements, 21,* 459-470. https://doi.org/10.1016/1359-0189(93)90185-C

Gallagher, Kerry, Brown, Roderick, Johnson, & Christopher. (1998). Fission track analysis and its applications to geological problems. *Annual Review of Earth & Planetary Sciences, 26,* 519-572. https://doi.org/10.1146/ANNUREV.EARTH.26.1.519

Gao, Y, G., Li, Y, H. (2014). Crustal thickness and Poisson's ratio in Northeast to North China and its geological significance. *Chinese Journal of Geophysics, 57,* 11.

Gleadow, A., Duddy, I.R., Green, P.F., & Lovering, J.F. (1986). Confined fission track lengths in apatite: a diagnostic tool for thermal his-

tory analysis. *Contributions to Mineralogy and Petrology, 94,* 405-415. https://doi.org/10.1007/BF00376334

Grebennikov, A.V., Khanchuk, A.I., Gonevchuk, V.G., & Kovalenko, S.V. (2016). Cretaceous and Paleogene granitoid suites of the Sikhote-Alin area (Far East Russia): Geochemistry and tectonic implications. *Lithos, 261,* 250-261. https://doi.org/10.1016/j.lithos.2015.12.020

Guo, Z.X., Shi, Y.P., Yang, Y.T., Jiang, S.Q., & Lin, L.B. (2018). Inversion of the Erlian Basin (NE China) in the early Late Cretaceous: Implications for the collision of the Okhotomorsk Block with East Asia. *Journal of Asian Earth Sciences, 154,* 49-66. https://doi.org/10.1016/j.jseaes.2017.12.007

Hu, S., Raza, A., Min, K., Kohn, B.P., Reiners, P.W., Ketcham, R.A., Wang, J., & Gleadow, A.J.W. (2006). Late Mesozoic and Cenozoic thermotectonic evolution along a transect from the north China craton through the Qinling orogen into the Yangtze craton, central China. *Tectonics, 25,* 0278-7407. https://doi.org/10.1029/2006TC001985

Hurford, A.J., & Green, P.F. (1983). The zeta age calibration of fission-track dating – ScienceDirect. *Chemical Geology, 41,* 285-317. https://doi.org/10.1016/S0009-2541(83)80026-6

Jang, L.W., Liu, Y. J., Feng, Z. Q., & Tang, C. (2018). Provenance and tectonic setting of the naked River Formation in the northern Daxinganling: evidence from geochemistry and detrital zircon chronology. *World Geology, 37,* 688-701.

Jahn, B.M., Wu, F., & Chen, B. (2000). Massive granitoid generation in Central Asia: Nd isotope evidence and implication for continental growth in the Phanerozoic. *Episodes, 23,* 82-92. https://doi.org/10.18814/epiiugs/2000/v23i2/001

Jahn, B.M., Wu, F.Y., Capdevila, R., Martineau, F., Zhao, Z.H., & Wang, Y.X. (2001, Highly evolved juvenile granites with tetrad REE patterns: the Woduhe and Baerzhe granites from the Great Xing'an Mountains in NE China. *Lithos, 59,* 171-198. https://doi.org/10.1016/S0024-4937(01)00066-4

Ketcham, R.A., Carter, A., Donelick, R.A., Barbarand, J., & Hurford, A.J.(2007). Improved modeling of fission-track annealing in apatite. *American Mineralogist, 92,* 799-810. https://doi.org/10.2138/am.2007.2281

Ketcham, R.A., Donelick, R.A., Balestrieri, M.L., & Zattin, M. (2009). Reproducibility of apatite fission-track length data and thermal history reconstruction. *Earth and Planetary Science Letters, 284,* 504-515. https://doi.org/10.1016/j.epsl.2009.05.015

Kravchinsky, V.A., Cogné, J.-P., Harbert, W.P., & Kuzmin, M.I. (2002). Evolution of the Mongol–Okhotsk Ocean as constrained by new palaeomagnetic data from the Mongol–Okhotsk suture zone, Siberia. *Geophysical Journal International, 148,* 34-57. https://doi.org/10.1046/j.1365-246x.2002.01557.x.

Li, J.Y. (2006). Permian geodynamic setting of Northeast China and

adjacent regions: closure of the Paleo-Asian Ocean and subduction of the Paleo-Pacific Plate. *Journal of Asian Earth Sciences, 26,* 207-224. https://doi.org/10.1016/j.jseaes.2005.09.001

Li, N., Zhao, Y.W., Gong, L.W., & Wang, J.L. (2020). The Late Cenozoic Volcanic Groups in the South Daxing'anling, NE China: Geology, Geochemistry, and Chronology. *Geological Society, London, Special Publications,* SP510-2020. https://doi.org/10.1144/SP510-2020-28

Li, S.C., Liu, Z.H., Xu, Z.Y., Li, G., & Zhang, C. (2015). Age and tectonic setting of volcanic rocks of the Tamulangou Formation in the Great Xing'an Range, NE China. *Journal of Asian Earth Sciences, 113,* 471-480. https://doi.org/10.1016/j.jseaes.2014.09.014

Li, X.M., Yang, X.Y., Xia, B., Gong, G.L., Shan, Y.H., Zeng, Q.S., Li, W., & Sun, W.D. (2011). Exhumation of the Dahinggan Mountains, NE China from the Late Mesozoic to the Cenozoic: New evidence from fission-track thermochronology. *Journal of Asian Earth Sciences, 42,* 123-133. https://doi.org/10.1016/j.jseaes.2011.04.014

Liu, W., Siebel, W., Li, X.J., & Pan, X.F. (2005). Petrogenesis of the Linxi granitoids, northern Inner Mongolia of China: constraints on basaltic underplating. *Chemical Geology, 219,* 5-35. https://doi.org/10.1016/j.chemgeo.2005.01.013

Liu, Y.J., Li, W.M., Feng, Z.Q., Wen, Q.B., Neubauer, F., & Liang, C.Y. (2017). A review of the Paleozoic tectonics in the eastern part of Central Asian Orogenic Belt. *Gondwana Research, 43,* 123-148. https://doi.org/10.1016/j.gr.2016.03.013

Liu, Z.H., Liu, H.J., Wang, P., Wu, X.M., Zhu, D.F., & Wan, C.B. (2009). Discovery of Compressional Structure in Wuerxun–Beier Sag in Hailar Basin of Northeastern China and Its Geological Significance. *Earth Science Frontiers, 16,* 138-146. https://doi.org/10.1016/s1872-5791(08)60087-1

Liu, Z.J., Wang, D.P., Liu, L., Liu, W.Z., Wang, P.J., Du, X.D., & Yang, G. (1993). Sedimentary Characteristics of the Cretaceous in the Songliao Basin. *Acta Geologica Sinica - English Edition, 6,* 167-180. https://doi.org/10.1111/j.1755-6724.1993.mp6002005.x.

Luo, X., Gong, S., Sun, F.J., Wang, Z.H., & Qi, J.S. (2017). Effect of volcanic activity on hydrocarbon generation: Examples in Songliao, Qinshui, and Bohai Bay Basins in China. *Journal of Natural Gas Science and Engineering, 38,* 218-234. https://doi.org/10.1016/j.jngse.2016.12.022

Ma, X.Y. (1987). Summary of the Lithospheric Dynamics in China. *Acta Geologica Sinica-English, 61,* 15-29. https://doi.org/10.1111/j.1755-6724.1987.mp61002002.x

Malcolm, & Sambridge. (1999). Geophysical inversion with a neighbourhood algorithm—I. Searching a parameter space. *Geophysical Journal International, 138,* 479-494.

Meng, Q.R. (2003). What drove late Mesozoic extension of the northern China–Mongolia tract?. *Tectonophysics, 369,* 155-174, https://doi.org/10.1016/S0040-1951(03)00195-1

Meng, Y.K., Xu, Z.Q., Xu, Y., & Ma, S.W. (2018). Late Triassic Granites From the Quxu Batholith Shedding a New Light on the Evolution of the Gangdese Belt in Southern Tibet. *Acta Geologica Sinica, 92,* 462-481. https://doi.org/10.1111/1755-6724.13537

Metelkin, D.V., Gordienko, I.V., & Klimuk, V.S. (2007). Paleomagnetism of Upper Jurassic basalts from Transbaikalia: new data on the time of closure of the Mongol-Okhotsk Ocean and Mesozoic intraplate tectonics of Central Asia. *Russian Geology and Geophysics, 48,* 825-834. https://doi.org/10.1016/j.rgg.2007.09.004

Miao, L.C., Fan, W.M., Zhang, F.Q., Liu, D.Y., Jian, P., Shi, G.H., Tao, H., & Shi, Y.R. (2004). Zircon SHRIMP geochronology of the Xinkailing-Kele complex in the northwestern Lesser Xing'an Range, and its geological implications. *Chinese Science Bulletin, 02,* 201-209.

Nie, F.J., Zhang, J., Yan, Z.B., Wang, Y.N., Li, M.G., Xia, F., Zhu, C.H., Wang, S.L., & Hu, J. (2018). Apatite fission track chronology of the health rock mass and the late Cretaceous exhalation events and uranium mineralization in the northern margin of North China [in Chinese with English abstract]. *Acta Geologica Sinica, 92,* 313-329.

Northrup, C.J., & Royden, L.H. (1995). Motion of the Pacific plate relative to Eurasia and its potential relation to Cenozoic extension. *Geology, 23,* 719–722. https://doi.org/10.1130/0091-7613(1995)023

Pang, Y.M., Guo, X.W., Zhang, X.H., Zhu, X.Q., Hou, F.H., Wen, Z.H., & Han, Z.Z. (2020). Late Mesozoic and Cenozoic tectono-thermal history and geodynamic implications of the Great Xing'an Range, NE China. *Journal of Asian Earth Sciences, 189,* 104–155. https://doi.org/10.1016/j.jseaes.2019.104155

Reiners, P.W., Zhou, Z., Ehlers, T.A., Changhai, X.U., Brandon, M.T., Donelick, R.A., & Nicolescu, S.(2003). Post-orogenic evolution of the Dabie-Shan, eastern China, from (U-Th)/He and fission-track thermochronology. *American Journal of Science, 303,* 489. https://doi.org/10.2475/ajs.303.6.489

Sambridge, M. (1999). Geophysical inversion with a neighbourhood algorithmII. Appraising the ensemble. *Geophysical Journal of the Royal Astronomical Society, 138,* 727-746

Safonova, I., Seltmann, R., Kröner, A., Gladkochub, D., Schulmann, K., Xiao, W., Kim, J., Komiya, T., & Sun, M. (2011). A new concept of continental construction in the Central Asian Orogenic Belt. *Episodes, 34,* 186-196. https://doi.org/10.18814/epiiugs/2011/v34i3/005

Safonova, I.Y., & Santosh, M.(2014). Accretionary complexes in the Asia-Pacific region: Tracing archives of ocean plate stratigraphy and tracking mantle plumes. *Gondwana Research, 25,* 126-158. https://doi.org/10.1016/j.gr.2012.10.008

Safonova, I.Y., Utsunomiya, A., Kojima, S., Nakae, S., Tomurtogoo, O., Filippov, A.N., & Koizumi, K. (2009). Pacific superplume-related oceanic basalts hosted by accretionary complexes of Central Asia, Russian Far East and Japan. *Gondwana Research, 16,* 587-608. https://doi.org/10.1016/j.gr.2009.02.008

Şengör, A.M.C., Natal'in, B.A., & Burtman, V.S. (1993). Evolution of the Altaid tectonic collage and Palaeozoic crustal growth in Eurasia. *Nature, 364,* 299-307. https://doi.org/10.1038/364299a0

Sharp, W.D., & Clague, D.A. (2006). 50-Ma Initiation of Hawaiian-Emperor Bend Records Major Change in Pacific Plate Motion. *Science, 313,* 1281-1284.

Sorokin, A., Yarmolyuk, V., Kotov, A., Sorokin, A., Kudryashov, N., & Jinyi, L. (2004). Geochronology of Triassic–Jurassic Granitoids in the Southern Framing of the Mongol–Okhotsk Foldbelt and the Problem of Early Mesozoic Granite Formation in Central and Eastern Asia. *Doklady Earth Sciences, 399,* 1091-1094.

Sorokin, A.A., Kotov, A.B., Kovach, V.P., Ponomarchuk, V.A., & Savatenkov, V.M. (2014). Sources of the Late Mesozoic magmatic associations in the northeastern part of the Amurian microcontinent. *Petrology, 22,* 65-76. https://doi.org/10.1134/S0869591113050068

Sorokin, A.A., Zaika, V.A., Kovach, V.P., Kotov, A.B., Xu, W., & Yang, H. (2020). Timing of closure of the eastern Mongol–Okhotsk Ocean: Constraints from U–Pb and Hf isotopic data of detrital zircons from metasediments along the Dzhagdy Transect. *Gondwana Research, 81,* 58-78. https://doi.org/10.1016/j.gr.2019.11.009

Stewart, R.J., & Brandon, M.T. (2004). Detrital-zircon fission-track ages for the "Hoh Formation": Implications for late Cenozoic evolution of the Cascadia subduction wedge. *Geological Society of America Bulletin, 116,* 60. https://doi.org/10.1130/b22101.1

Stockli, D.F. (2005). Application of Low-Temperature Thermochronometry to Extensional Tectonic Settings. *Reviews in Mineralogy and Geochemistry, 58,* 411-448.

https://doi.org/10.2138/rmg.2005.58.16

Sun, C., Tang, J., Xu, W.L., Li, Y., & Zhao, S. (2017). Crustal accretion and reworking processes of micro-continental massifs within orogenic belt: A case study of the Erguna Massif, NE China. *Science China Earth Sciences, 60,* 1256-1267. https://doi.org/10.1007/s11430-016-9033-5

Sun, D.Y., Gou, J., Wang, T.H., Ren, Y.S., Liu, Y.J., Guo, H.Y., Liu, X.M., & Hu, Z.C. (2013). Geochronological and geochemical constraints on the Erguna massif basement, NE China – subduction history of the Mongol–Okhotsk oceanic crust. *International Geology Review, 55,* 1801-1816. https://doi.org/10.1080/00206814.2013.804664

Suo, Y.H., Li, S.Z., Cao, X.Z., Wang, X.Y., Somerville, I., Wang, G.Z., Wang, P.C., & Liu, B. (2020). Mesozoic-Cenozoic basin inversion and geodynamics in East China: A review. *Earth-Science Reviews, 210,* 103357. https://doi.org/10.1016/j.earscirev.2020.103357

Szymanski, E., Stockli, D.F., Johnson, P.R., & Hager, C. (2016). Thermochronometric evidence for diffuse extension and two-phase rifting within the Central Arabian Margin of the Red Sea Rift. *Tectonics, 35,* 2863-2895. https://doi.org/10.1002/2016tc004336

Tang, J., Xu, W.L., Wang, F., Zhao, S., & Wang, W. (2016). Early Mesozoic southward subduction history of the Mongol–Okhotsk oceanic plate: Evidence from geochronology and geochemistry of Early Mesozoic intrusive rocks in the Erguna Massif, NE China. *Gondwana Research, 31,* 218-240. https://doi.org/10.1016/j.gr.2014.12.010

Tang, Z.Y., Sun, D.Y., Mao, A.Q., Yang, D.G., Deng, C.Z., & Liu, Y. (2018). Timing and evolution of Mesozoic volcanism in the central Great Xing'an Range, northeastern China. *Geological Journal, 54,* 3737-3754. https://doi.org/10.1002/gj.3366

Tomurtogoo, O., Windley, B.F., Kroner, A., Badarch, G., & Liu, D.Y.(2005). Zircon age and occurrence of the Adaatsag ophiolite and Muron shear zone, central Mongolia: constraints on the evolution of the Mongol-Okhotsk ocean, suture and orogen. *Journal of the Geological Society, 162,* 125-134. https://doi.org/10.1144/0016-764903-146

Vermeesch, P. (2009). RadialPlotter: A Java application for fission track, luminescence and other radial plots. *Radiation Measurements, 44,* 409-410. https://doi.org/10.1016/j.radmeas.2009.05.003

Vermeesch, P. (2012). On the visualisation of detrital age distributions. *Chemical Geology, 312-313,* 190-194. https://doi.org/10.1016/j.chemgeo.2012.04.021

Wang, F., Zhou, X. H., Zhang, L. C., Ying, J. F., Zhang, Y. T., Wu, F. Y., & Zhu, R. X. (2006). Late Mesozoic volcanism in the Great Xing'an Range (NE China): Timing and implications for the dynamic setting of NE Asia. *Earth and Planetary Science Letters, 251,* 179-198. https://doi.org/10.1016/j.epsl.2006.09.007

Wang, S.J., Hu, J.W., Yan, J.H., Li, F., Chen, N.S., Tang, Q., Guo, B.C., & Zhan, L.F. (2019). Assessment of Geothermal Resources in Petroliferous Basins in China. *Mathematical Geosciences, 51,* 271-293. https://doi.org/10.1007/s11004-019-09786-9

Wang, S.Y., Cheng, Y.H., Xu, D.H., Miao, P.S., Jin, R.S., Zhang, T.F., Xu, Z.L., Cheng, X.Y., Zhao, L., Li, C.H., & Zhang, X.W. (2020a). Late Cretaceous-Cenozoic tectonic-sedimentary evolution and U-enrichment in the southern Songliao Basin. *Ore Geology Reviews, 126,* 103786, https://doi.org/10.1016/j.oregeorev.2020.103786

Wang, S.Y., Cheng, Y.H., Zeng, L., Miao, P.S., Jin, R.S., Zhang, T.F., Li, C.H., & Zhang, X.W. (2020b) Thermal imprints of Cenozoic tectonic evolution in the Songliao Basin, NE China: Evidence from apatite fission-track (AFT) of CCSD-SK1 borehole. *Journal of Asian Earth Sciences, 195,* 104353. https://doi.org/10.1016/j.jseaes.2020.104353

Wang, T., Guo, L., Zhang, L., Yang, Q.D., Zhang, J.J., Tong, Y., & Ye, K. (2015). Timing and evolution of Jurassic–Cretaceous granitoid magmatisms in the Mongol–Okhotsk belt and adjacent areas, NE Asia: Implications for transition from contractional crustal thickening to extensional thinning and geodynamic settings. *Journal of Asian Earth Sciences, 97,* 365-392. https://doi.org/10.1016/j.jseaes.2014.10.005

Wang, T., Tong, Y., Wang, X.X., Mao, J.R., Zhang, H.R., Huang, H., Li, S., Guo, L., & Zhang, J.J.(2018). Some progress on understanding the Phanerozoic granitoids in China. *China Geology, 1,* 84-108. https://doi.org/10.31035/cg2018010

Wang, T., Zheng, Y.D., Zhang, J.J., Zeng, L.S., Donskaya, T., Guo, L., & Li, J.B. (2011). Pattern and kinematic polarity of late Mesozoic extension in continental NE Asia: Perspectives from metamorphic core complexes. *Tectonics, v. 30,* TC6007. https://doi.org/10.1029/2011TC002896

Wei, C.S., Zheng, Y.F., Zhao, Z.F., & Valley, J. (2002). Oxygen and neodymium isotope evidence for recycling of juvenile crust in Northeast China. *Geology, 30,* 375-378. https://doi.org/10.1130/0091-7613(2002)030

Wilde, S.A. (2015). Final amalgamation of the Central Asian Orogenic Belt in NE China: Paleo-Asian Ocean closure versus Paleo-Pacific plate subduction — A review of the evidence. *Tectonophysics, 662,* 345-362. https://doi.org/10.1016/j.tecto.2015.05.006

Wu, F.Y., Lin, J.Q., Wilde, S.A., Zhang, X., & Yang, J.H. (2005) Nature and significance of the Early Cretaceous giant igneous event in eastern China. *Earth and Planetary Science Letters, 233,* 103-119. https://doi.org/10.1016/j.epsl.2005.02.019

Wu, F.Y., Sun, D.Y., Ge, W.C., Zhang, Y.B., Grant, M.L., Wilde, S.A., & Jahn, B. (2011). Geochronology of the Phanerozoic granitoids in northeastern China. *Journal of Asian Earth Sciences, 41,* 1-30. https://doi.org/10.1016/j.jseaes.2010.11.014

Wu, F.Y., Zhao, G.C., Sun, D.Y., Wilde, S.A., & Yang, J.H. (2007). The Hulan Group: Its role in the evolution of the Central Asian Orogenic Belt of NE China. *Journal of Asian Earth Sciences, 30,* 542-556. https://doi.org/10.1016/j.jseaes.2007.01.003

Wu, H.H., Hu, D.G., Wu, X.W., You, B.J., Chang, P.Y., & zhang, M. (2016). Apatite fission track evidence of mesozoic-Cenozoic uplift and exhalation in

the northern part of the Greater Hinggan Mountains [in Chinese with English abstract]. *Geological Bulletin Of China, 35,* 2058-2062.

Xiang, C.F., Feng, Z.Q., Pang, X.Q., Wu, H.Y., & Li, J.H. (2007). Late stage thermal history of the Songliao Basin and its tectonic implications: Evidence from apatite fission track (AFT) analyses: Science in China Series D. *Earth Sciences, 50,* 1479-1487. https://doi.org/10.1007/s11430-007-0104-y

Xiao, W.J., Windley, B., Hao, J.J., & Zhai, M.G. (2003). Accretion Leading to Collision and the Permian Solonker Suture, Inner Mongolia, China: Termination of the Central Asian Oragenic Belt: Termination of the Central Asian Orogenic Belt. *Tectonics, 22,* 1069-1088. https://doi.org/10.1029/2002TC001484

Xiong, X.S., Gao, R., Li, Y.K., Hou, H.S., Liang, H.D., Li, W.H., Guo, L.H., & Lu, Z.W. (2015). The lithosphere structure of the Great Xing'an Range in the eastern Central Asian Orogenic Belt: Constrains from the joint geophysical profiling. *Journal of Asian Earth Sciences, 113,* 481-490. https://doi.org/10.1016/j.jseaes.2015.06.006

Xu, W.L., Chen, J.H., Weng, A.H., Tang, J., Wang, F., Wang, C.G., Guo, P., Wang, Y.N., Yang, H., &d Sorokin, A.A. (2020). Stagnant slab front within the mantle transition zone controls the formation of Cenozoic intracontinental high-Mg andesites in northeast Asia. *Geology, 49,* 19-24. https://doi.org/10.1130/g47917.1

Xu, W.L., Pei, F.P., Wang, F., Meng, E., Ji, W.Q., Yang, D.B., & Wang, W. (2013). Spatial–temporal relationships of Mesozoic volcanic rocks in NE China: Constraints on tectonic overprinting and transformations between multiple tectonic regimes. *Journal of Asian Earth Sciences, 74,* 167-193. https://doi.org/10.1016/j.jseaes.2013.04.003

Yang, Q.D., Guo, L., Wang, T., Zeng, T., Zhang, L., Tong, Y., Shi, X.J., & Zhang, J.J. (2014). Age, genesis, provenance and tectonic setting of late Mesozoic granites in Ganjuermiao area in the middle and southern part of the Greater Hinggan Mountains [in Chinese with English abstract]. *Journal of rock, 030,* 1961-1981.

Yang, Y.T., Guo, Z.X., Song, C.C., Li, X.B., & He, S. (2015). A short-lived but significant Mongol–Okhotsk collisional orogeny in latest Jurassic–earliest Cretaceous. *Gondwana Research, 28,* 1096-1116. https://doi.org/10.1016/j.gr.2014.09.010

Zeng, T., Wang, T., Guo, L., Tong, Y., Zhang, J.J., Shi, X.J., Zhang, L., & Li, Y.F. (2011). Age, genesis and geological significance of late Mesozoic granitoids in Xinkailing area, northeast China [in Chinese with English abstract]. *Journal of Jilin University (Earth Science Edition), 41,* 1881-1900.

Zhang, F.Q., Chen, H.L., Yu, X., Dong, C.W., Yang, S.F., Pang, Y.M., & Batt, G.E. (2011). Early Cretaceous volcanism in the northern Songliao Basin,

NE China, and its geodynamic implication. *Gondwana Research, 19,* 163-176. https://doi.org/10.1016/j.gr.2010.03.011

Zhang, F.Q., Dilek, Y., Chen, H.L., Yang, S.F., & Meng, Q.A.(2017). Late Cretaceous tectonic switch from a Western Pacific- to an Andean-Type continental margin evolution in East Asia, and a foreland basin development in NE China. *Terra Nova, 29,* 335-342. https://doi.org/10.1111/ter.12286

Zhang, J.H., Ge, W.C., Wu, F.Y., Wilde, S.A., Yang, J.H., & Liu, X.M. (2008). Large-scale Early Cretaceous volcanic events in the northern Great Xing'an Range, Northeastern China. *Lithos, 102,* 138-157. https://doi.org/10.1016/j.lithos.2007.08.011

Zhang, L.Y., Li, S.C., Chu, X.L., & Shang, Y.M. (2019). Early Cretaceous Adakitic Rocks in the Northern Great Xing'an Range, NE China: Implications for the Final Closure of Mongol-Okhotsk Ocean and Regional Extensional Setting. *Acta Geologica Sinica - English Edition, 93,* 1544-1558. https://doi.org/10.1111/1755-6724.14362

Zhang, X.D., Yu, Q., Chen, F.J., & Wang, X.W. (2000). Structural characteristics and formation of metamorphic core complex and extensional fault depression in Songliao Basin [in Chinese with English abstract]. *Earth Science Frontiers (China University of Geosciences,Beijing), 7,* 411-419.

Zhao, H.B., Mo, X.X., Xu, S.M., Li, S.L., & Ma, B.Y. (2007). Composition and evolution of metamorphic core complex in Xinkailing, Heilongjiang province [in Chinese with English abstract]. *Chinese Journal Of Geology, 42,* 176-188.

Zhao, L., Jia, R.F., Qin, J.Z., & Guo, A.M. (1998). Study on thermal evolution history of Jurassic strata in Erlian Basin [in Chinese with English abstract]. *Geochimica, 27,* 592-598.

Zuo, Y.H., Qiu, N.S., Hao, Q.Q., Pang, X.Q., Guo, X., Wang, X.J., Luo, X.P., & Zhao, Z.Y. (2015). Geothermal regime and source rock thermal evolution in the Chagan Sag, Inner Mongolia, Northern China. *Marine and Petroleum Geology, 59,* 245–267. https://doi.org/10.1016/j.marpetgeo.2014.09.001

Zuo, Y.H., Wang, C.C., Tang, S.L., & Hao, Q.Q. (2016). Mesozoic and Cenozoic thermal history and source rock thermal evolution of the Baiyinchagan sag, Erlian Basin, Northern China. *Journal of Petroleum Science and Engineering, 139,* 171-184. https://doi.org/10.1016/j.petrol.2015.12.025